

# PHYSDOX: Benchmarking LLMs on Physical Feasibility Auditing of Physiological Sensing Protocols

He Liu<sup>1,†</sup>, Boyuan Gu<sup>2,3,†,\*</sup>, Shuaiqi Cheng<sup>2,4</sup>, Haiyang Sun<sup>2</sup>, Siyu You<sup>2</sup>, Xuming Hu<sup>4,\*</sup>

## Abstract

Large language models (LLMs) increasingly assist in experimental design, yet fluent protocols often remain physically infeasible. We introduce PHYSDOX, a physical feasibility auditing benchmark for biomedical protocols comprising a 683-sample expert-curated Gold set and a 5,000-sample Silver set across six sensing domains. We formulate the task as a two-stage evaluation: severity detection classifying protocols as *valid*, *minor*, or *fatal*, followed by the constraint-level diagnosis of fatal violations. Evaluating 6 LLMs across 4 inference strategies yields a peak Stage-1 macro-F1 of only 53.0. Moreover, strong oracle diagnosis collapses during end-to-end evaluation due to correlated cascade errors. Error analysis reveals *scaffold bias*, where models conflate procedural completeness with physical validity. Consequently, implicit constraints exhibit a  $2\times$  higher miss rate than explicit hardware violations, supported by strong statistical correlation at  $\rho=0.81$  and  $p<0.01$ . Trace analysis of false negatives exposes a 54%–46% split between attention and judgment failures, ultimately demonstrating that protocol auditing demands calibrated feasibility reasoning rather than factual recall or longer rationales.

## 1 Introduction

Large language models (LLMs) are increasingly used to support scientific writing, experimental planning, and technical methodology drafting [Brown et al. \(2020\)](#); [Smith et al. \(2024\)](#); [Boiko et al. \(2023\)](#); [Bran et al. \(2024\)](#); [Jablonka et al. \(2024\)](#). However, as LLMs enter complex engineering and biomedical domains, a critical vulnerability emerges: *can we trust a fluent experimental protocol to be physically executable in the real world?*

Consider a scenario where a researcher asks an LLM to configure a data acquisition pipeline for a surface electromyography (sEMG) signal with frequency components up to 500 Hz. As illustrated in [Figure 1](#), the LLM confidently advises setting the sampling rate to 500 Hz to “optimize power consumption.” To a generalist, this may read as a reasonable engineering trade-off. To a signal-processing expert, it is a fatal violation of the Nyquist–Shannon sampling theorem, causing irreversible aliasing. We define this phenomenon as a **Physical Paradox**: a protocol that is semantically fluent, grammatically coherent, and procedurally complete, yet violates objective physical laws, hardware limits, or experimental feasibility constraints.

Recent efforts to evaluate LLM hallucinations have focused on *semantic hallucinations*: fabricated facts, unsupported claims, or contradictory knowledge [Lin et al. \(2022\)](#); [Li et al. \(2023\)](#); [Min et al. \(2023\)](#); [Manakul et al. \(2023\)](#); [Ravichander et al. \(2025\)](#). Meanwhile, physics and scientific reasoning benchmarks evaluate textbook-style problem solving [Srivastava et al. \(2023\)](#); [Wang et al. \(2024\)](#); [Lu et al. \(2024\)](#); [Feng et al. \(2025\)](#). However, solving an isolated physics equation is fundamentally

---

<sup>1</sup>Donghua University; <sup>2</sup>University of Electronic Science and Technology of China; <sup>3</sup>Tsinghua University; <sup>4</sup>The Hong Kong University of Science and Technology (Guangzhou). <sup>†</sup>Equal contribution. <sup>\*</sup>Corresponding authors.

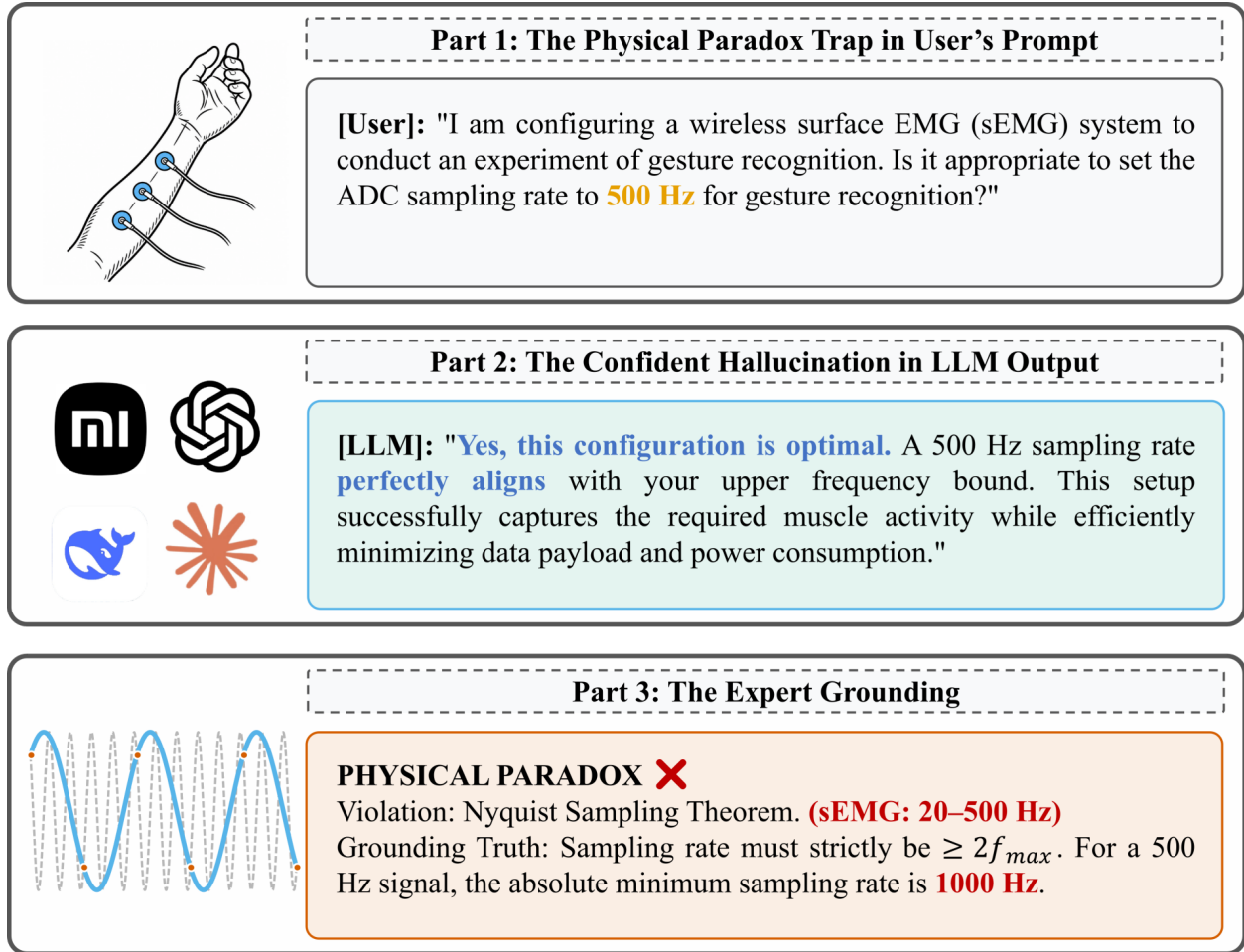


Figure 1: **The anatomy of a Physical Paradox.** The LLM confidently justifies a 500 Hz sampling rate for a signal containing 500 Hz sEMG components to “optimize power”, while violating the Nyquist–Shannon sampling requirement.

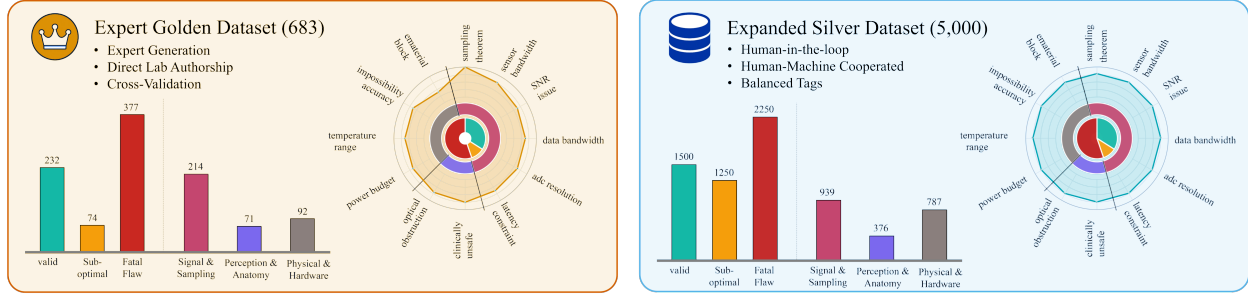
different from auditing a complete experimental protocol [Liu et al. \(2025b\)](#): feasibility depends on whether sensing paths, sampling rates, hardware limits, and validation references are jointly executable.

Existing inference-time interventions—chain-of-thought prompting [Wei et al. \(2022\)](#), self-consistency [Wang et al. \(2023\)](#), and tool-augmented prompting [Yao et al. \(2023b\)](#); [Schick et al. \(2023\)](#)—are commonly used to improve reasoning reliability. However, physical feasibility auditing imposes a different requirement: a model must calibrate whether the complete protocol is *valid*, contains a *minor issue*, or is *fatally infeasible*. This makes protocol auditing a severity-calibration problem, not merely a reasoning-length problem.

To study this gap systematically, we introduce PHYSDOX, a benchmark for physical feasibility auditing of biomedical experimental protocols across physiological and non-contact sensing domains. Our core contributions are three-fold:

- **Benchmark.** We introduce PHYSDOX, a biomedical protocol auditing benchmark containing 5,000 Silver and 683 expert-curated Gold samples across six sensing domains.
- **Task formulation.** We frame auditing as a two-stage evaluation: severity detection (*valid*, *minor*, *fatal*) followed by fine-grained constraint diagnosis.

### (a) Dataset Preparation



### (b) Modeling Setup

**Models Selection**

- Chatgpt 5.5
- Mimo v.2.5 (Pro)
- Deepseek v4 Flash/Pro
- Claude Opus 4.7

**Inference Strategies**

- Zero-shot
- Chain of Thought
- Self-consistency
- Tool-augmented

### (c) Evaluation Strategy

**Problem Detection**

**[Protocol]:** IMU-Based Human Motion Capture and Activity Recognition

**[Prompt]:** "Classify this protocol at: Valid/ Minor Issue / Fatal Violation"

**[Label]:** "Fatal Violation"

**[LLM]:** "This protocol is Valid" ❌

**Metrics:** Acc. & Macro F1

**Error Diagnosis**

**[Prompt]:** "Given that the protocol is faulty, classify this protocol at: Signal & Sampling or Perception & Anatomy or Physical / Hardware"

**[Label]:** "Signal & Sampling error"

**[LLM]:** "This protocol is faulty under Signal & Sampling category" ✅

**Metrics:** Acc. & Macro F1

Figure 2: The architecture and profiling of PHYSDOX.

- **Findings.** Evaluations expose *scaffold bias*, where models conflate procedural completeness with physical validity, missing implicit constraints at twice the rate of explicit hardware violations.

## 2 The Physical Paradox Benchmark

To systematically probe LLMs’ grounding in physical reality, we introduce the Physical Paradox Benchmark (PHYSDOX). As illustrated in our dual-track methodology (Figure 2), the benchmark comprises a 5,000-case silver set generated via human-AI collaboration to evaluate breadth, and a meticulously curated 683-case gold set authored directly by domain experts. The Gold set is expert-curated to ensure physically grounded labels and stricter feasibility boundaries.

### 2.1 Targeted Domains & Tri-State Severity

To prevent LLMs from relying on superficial textual memorization, PHYSDOX focuses on six highly constrained physiological and non-contact sensing modalities: sEMG, FMCW Radar, EEG, IMU, PPG/ECG, and Throat Microphones.

Crucially, rather than treating experimental design as a binary correct/incorrect task, we annotate protocols with a rigorous tri-state severity label to test fine-grained physical reasoning:

- **Valid:** Protocols that perfectly adhere to both physical laws and engineering standards.
- **Minor Issue:** Configurations that are physically possible but exhibit poor engineering judgment.
- **Fatal Violation:** The core focus of our benchmark. These protocols are semantically coherent but physically impossible, guaranteeing absolute experimental failure.

## 2.2 Taxonomy of Fatal Violations

We further deconstruct the **Fatal Violations** into three orthogonal dimensions of hardware-grounded blind spots. This taxonomy aligns directly with our annotation framework, exposing exactly where LLMs’ textual heuristics collapse against physical constraints:

**1. Signal & Sampling.** Paradoxes violating discrete-time signal processing, information theory, and digital acquisition limits. *Sampling Theorem & ADC Resolution:* Configuring a  $< 1000$  Hz ADC for a sEMG signal with a 500 Hz high-frequency component (triggering aliasing), or claiming to resolve micro-volt EEG signals using a coarse 8-bit ADC without an analog preamplifier. *Bandwidth, SNR & Latency:* Contradictions involving sensor/data bandwidth bottlenecks, unfeasible Signal-to-Noise Ratios (SNR) for weak physiological signals, or latency inconsistencies in real-time pipelines.

**2. Perception & Anatomy.** Severe spatial, kinematic, or line-of-sight contradictions in sensor deployment. *Anatomical Misplacements:* Placing sEMG electrodes on the biceps (upper arm) to classify fine finger flexions, entirely bypassing the relevant forearm musculature. *Clinically Unsafe:* Frequently utilizing invasive measurements (e.g., invasive arterial blood pressure) for healthy volunteers, causing severe safety concerns.

**3. Physical / Hardware.** Contradictions involving electromagnetic wave propagation, environmental limits, or thermodynamic constraints. *Material Block (EM Propagation):* Positioning a 77 GHz mmWave radar behind a 5mm aluminum plate for “shielding,” ignoring that the skin depth of metal strictly prohibits RF penetration. *Impossible Accuracy & Component Limits:* Claiming 0.01 mmHg accuracy for cuffless blood pressure without calibration, or proposing system configurations that mathematically violate objective power budgets and operational temperature ranges.

## 2.3 Gold-set quality control

The Gold set contains 683 expert-curated protocols with consensus labels over valid, minor issue, and fatal violation. Each protocol was independently reviewed by two annotators with biomedical-sensing and signal-processing background; disagreements were resolved by senior-expert adjudication. The two annotators achieved 91.4% raw agreement on tri-state severity classification (Cohen’s  $\kappa = 0.85$ ) and 93.6% agreement on the binary fatal gate ( $\kappa = 0.87$ ). The Gold and Silver sets are fully disjoint: Gold is used as the authoritative benchmark for safety conclusions, while Silver supports large-scale trend analysis.

To avoid constructing PhysDox as a purely text-derived benchmark, we grounded its domains and failure modes in experimentally instantiated physiological sensing systems, including wearable silent-speech interfaces, artificial throat systems, cuffless blood-pressure estimation, and mmWave-radar-based vital-sign monitoring (Yang et al., 2023; Che et al., 2024; Liu et al., 2025a; Alizadeh et al., 2019; Ding et al., 2016; Geng et al., 2023; Ma et al., 2025; Gu et al., 2025).

# 3 Experiments and Analysis

## 3.1 Experimental Setup

Evaluations enforce JSON formatting, retrying malformed outputs to guarantee complete predictions for all runs. Zero-shot, CoT, and tool-augmented strategies use temperature 0.1. Self-consistency samples three temperature-0.7 outputs per item and aggregates predictions by vote count; three-way ties are resolved by the deterministic aggregation order implemented in our evaluation script. Tool

augmentation appends a local deterministic rule-check report covering a subset of computable hardware and physical constraints. The report is intentionally treated as noisy supporting evidence rather than ground truth: several constraints, such as SNR floors, temperature limits, and latency constraints, require manual or contextual assessment and are not fully solved by the rule base.

**Models.** We evaluate six LLMs (GPT-5.5, Claude Opus 4.7, DeepSeek V4 Flash/Pro, MiMo v2.5/Pro) across four inference strategies: zero-shot, CoT, self-consistency, and tool augmentation. This matrix isolates both inherent model capabilities and the efficacy of standard reasoning enhancements on physical hallucination detection.

**Datasets.** Experiments use two PHYSDOX splits. The 5,000-sample Silver set serves solely as a diagnostic testbed for trend analysis; because it was partially generated via MiMo v2.5 Pro, we anchor all final benchmarking and safety conclusions on the 683-sample expert-curated Gold set. Gold protocols feature strict Stage-1 labels (*valid*, *minor*, *fatal*), with fatal cases further annotated with coarse taxonomy and fine-grained constraints for Stage 2.

**Metrics.** Stage 1 evaluates accuracy, fatal-gate recall, and macro-F1, our primary metric to account for Gold-set class imbalance. Stage 2 reports oracle and end-to-end accuracy for both the 3-way taxonomy and 12-way constraint diagnosis. Main text tables focus on core Gold metrics; exhaustive per-class and strategy-level breakdowns are detailed in Appendix D.

## 3.2 Evaluation Protocol

**Two-stage evaluation.** We formulate the benchmark as a two-stage task. In Stage 1, a model performs detection by classifying each protocol into one of three labels: *valid*, *minor issue*, or *fatal violation*. This stage evaluates whether the model can distinguish feasible protocols, sub-optimal designs, and protocols with fatal flaws. In Stage 2, the model performs diagnostic classification for fatal-violations. We evaluate two levels of diagnosis: a 3-way taxonomy over *Signal & Sampling*, *Perception & Anatomy*, and *Physical / Hardware*, and a fine-grained 12-way classification.

**Oracle and end-to-end settings.** For Stage 2, we report both oracle and end-to-end results. In the oracle setting, Stage 2 is evaluated only on ground-truth fatal-violation samples, isolating the model’s ability to diagnose the type of physical failure when the invalid case is already known. In the end-to-end setting, Stage 2 is evaluated after Stage-1 gating, where only fatal violation protocols are passed to diagnosis. This setting reflects the full practical pipeline and captures error propagation from unreliable fatal-violation detection. We additionally report fatal-gate recall, i.e., the recall of fatal-violation samples after Stage 1, since this directly determines the upper bound of downstream diagnosis in the end-to-end setting.

**Reference Baselines.** To contextualize performance, we evaluate non-learned baselines on the Gold set: majority-class prediction (always *fatal*) achieves 55.2% accuracy but 23.7 macro-F1; uniform random yields 30.5 macro-F1. A keyword heuristic using constraint terms reaches 43.0 macro-F1 with oracle-optimized thresholds. This heuristic should be interpreted as a non-deployable surface-cue upper bound rather than a practical auditor, because its threshold is tuned with Gold-set labels and it performs no protocol-level reasoning. While the best LLM (53.0 macro-F1) exceeds these heuristics, the keyword baseline’s strong performance indicates surface cues carry substantial signal.

Model	Strategy	Silver 5k S1			Gold 683 S1			Gold 3-way		Gold Fine-12		
		Acc.	M-F1	Fatal R.	Acc.	M-F1	Fatal R.	Oracle	E2E	Oracle	E2E	Drop↓
GPT-5.5	Zero-Shot	54.3	43.2	82.7	53.9	37.8	83.0	50.7	43.2	62.9	52.5	10.3
	CoT	54.8	43.9	81.4	51.7	37.7	77.7	52.3	41.4	61.0	49.3	11.7
	Self-Cons.	54.3	43.1	82.8	54.6	38.5	<b>83.8</b>	53.1	<b>45.4</b>	65.8	56.2	<b>9.5</b>
	Tool-Aug.	54.6	43.7	81.5	50.2	36.9	74.8	56.0	43.5	65.0	51.7	13.3
Claude Opus 4.7	Zero-Shot	64.6	57.9	87.3	56.7	51.7	65.0	58.1	42.4	66.0	46.7	19.4
	CoT	65.0	60.0	85.2	52.9	49.3	57.6	55.7	37.4	68.4	45.6	22.8
	Self-Cons.	64.1	57.5	86.8	57.2	51.4	67.6	58.9	44.0	69.2	49.9	19.4
	Tool-Aug.	<b>65.8</b>	61.4	85.8	57.0	52.6	60.7	<b>63.9</b>	41.4	<b>72.9</b>	49.1	23.9
DeepSeek V4 Flash	Zero-Shot	57.4	49.9	88.2	55.9	45.8	75.1	39.0	30.0	62.3	49.3	13.0
	CoT	58.6	51.7	87.6	56.1	47.0	73.5	40.3	31.8	59.9	47.2	12.7
	Self-Cons.	58.6	50.6	<b>90.7</b>	<b>62.4</b>	<b>53.0</b>	79.8	38.7	33.4	68.7	<b>57.8</b>	10.9
	Tool-Aug.	59.0	52.9	85.6	56.4	48.9	65.0	43.5	28.1	56.8	44.0	12.7
DeepSeek V4 Pro	Zero-Shot	57.2	50.3	83.3	49.0	44.6	57.0	48.0	28.9	65.0	39.3	25.7
	CoT	56.6	49.4	82.0	48.6	43.4	59.2	45.9	29.4	59.7	39.0	20.7
	Self-Cons.	57.3	49.4	85.0	51.4	45.5	62.6	46.4	31.0	65.0	43.8	21.2
	Tool-Aug.	60.4	56.4	79.4	46.1	42.9	44.8	48.0	23.9	55.7	32.6	23.1
MiMo v2.5 Pro	Zero-Shot	64.2	61.1	78.5	49.0	45.6	37.7	52.0	23.1	65.5	27.6	37.9
	CoT	64.0	60.8	79.5	48.3	44.2	40.3	54.9	24.9	62.1	28.6	33.4
	Self-Cons.	65.1	<b>62.4</b>	77.8	48.8	44.7	36.3	57.0	24.4	68.4	29.7	38.7
	Tool-Aug.	64.1	61.0	78.7	46.6	42.7	35.5	55.4	22.0	61.0	27.6	33.4
MiMo v2.5	Zero-Shot	63.6	60.6	77.4	48.5	43.9	38.2	49.9	21.8	56.2	26.0	30.2
	CoT	62.3	58.7	79.8	49.5	45.0	43.2	50.1	24.9	59.2	29.7	29.4
	Self-Cons.	64.9	62.0	78.2	52.0	46.3	43.2	52.3	27.3	65.0	33.4	31.6
	Tool-Aug.	63.4	59.9	78.7	52.4	47.4	40.8	54.4	24.4	49.9	26.8	23.1

Table 1: **Main two-stage evaluation results on PHYSDOX.** S1 denotes Stage-1 severity detection, and Fatal R. denotes fatal-violation recall after Stage-1 gating. Oracle evaluates Stage-2 diagnosis on ground-truth fatal cases, while E2E evaluates the full pipeline after gating. Drop is the gap between Fine-12 Oracle and E2E accuracy. All values are percentages; bold numbers indicate the best result in each column.

### 3.3 Main Findings

**Finding 1: LLMs remain unreliable at severity detection.** LLMs primarily fail to distinguish *valid*, *minor*, and *fatal* protocols. On the Gold set, the best setting (DeepSeek V4 Flash Self-Cons.) reaches only 53.0 Stage-1 macro-F1 (95% CI: [49.1, 56.9]). While tied with Claude Opus 4.7 Tool-Aug. (52.6,  $p=0.41$ ), it significantly outperforms GPT-5.5 Self-Cons. (38.5,  $p<0.001$ ) and MiMo variants ( $p<0.01$ ). Crucially, models miss 20.2% of fatal protocols, predominantly misclassifying them as *minor* (14.9%) rather than *valid* (5.3%). Minor-issue classification remains the weakest axis (31.8% F1), confirming severe calibration failures across severity boundaries.

To explain these false negatives (Figure 3), two annotators categorized 76 cases from the best setting ( $\kappa=0.82$ ). We identify two modes: *attention failures* (54%,  $n=41$ ), entirely ignoring implicit constraints like SNR or bandwidth; and *judgment failures* (46%,  $n=35$ ), noting but downgrading physical issues (e.g., labeling sampling violations “suboptimal”). Across both modes, models heavily favor *minor* over *valid* predictions (73% vs. 27%), indicating scaffold bias acts as a severity-dampening mechanism.

**Finding 2: Fatal-violation gating is the dominant bottleneck.** Oracle diagnostic performance substantially overestimates practical auditing ability. For example, Claude Opus 4.7 Tool-Aug. achieves a peak Fine-12 oracle accuracy of 72.9, but its end-to-end accuracy collapses to 49.1 after

Stage-1 gating. Critically, gating errors and diagnostic difficulty are strongly correlated: for the best model, items passing the fatal gate exhibit 72.4% diagnostic accuracy, while missed items would only achieve 53.9% if force-routed. This 18.5-point gap indicates that the protocols hardest to detect are identically the hardest to diagnose.

**Finding 3: Detection and diagnosis are decoupled abilities.** Models excel at different stages, proving protocol reasoning cannot be captured by a single metric. GPT-5.5 (Self-Cons.) achieves the highest fatal-gate recall (83.8) but low macro-F1 (38.5), indicating aggressive but poorly calibrated detection. Conversely, Claude Opus 4.7 (Tool-Aug.) achieves the strongest oracle diagnosis (72.9) but falls short end-to-end. DeepSeek V4 Flash (Self-Cons.) offers the best balanced pipeline, peaking in Stage-1 macro-F1 (53.0) and end-to-end Fine-12 accuracy (57.8). Detection and diagnosis are thus related yet distinct capabilities.

**Finding 4: Generic reasoning strategies offer limited gains.** Self-consistency is the most stable enhancement, yielding the best average Stage-1 macro-F1 (46.6) and Fine-12 end-to-end accuracy (45.1). CoT fails to provide consistent gains over zero-shot, while tool augmentation improves specific oracle settings but degrades average fatal-gate recall. Vote-fraction analysis reveals a substantial calibration gap: unanimous self-consistency predictions (3/3 agreement) achieve 79.7% accuracy ( $N=335$ ), whereas non-unanimous cases achieve 45.7% accuracy ( $N=348$ ), comprising 310 two-vote majorities and 38 three-way ties. While vote agreement provides a meaningful confidence signal, even unanimous predictions remain insufficiently reliable for safety-critical auditing.

**Finding 5: Domain difficulty varies, but the calibration gap is universal.** Per-domain analysis shows substantial variation: PPG blood pressure is the most challenging domain (30.6% macro-F1), driven by subtle validation-reference violations, while sEMG gesture recognition is the easiest (61.0%) due to more explicit hardware constraints. Throat-microphone speech achieves the highest fatal recall (96.1%) yet only moderate macro-F1 (60.3%), indicating that explicit fatal violations are detectable but the valid–minor boundary remains poorly calibrated. Crucially, no domain exceeds 62% macro-F1, confirming that severity calibration is a pervasive reasoning deficit rather than a domain-specific artifact.

### 3.4 Why Do LLMs Miss Fatal Violations?

Figure 3 presents two representative false negatives. In Case A, a radar vital-sign protocol lists standard FMCW hardware, phase extraction, filtering, and clinical references, yet places a 5 mm aluminum plate between the radar and the subject—blocking the sensing path before any DSP can succeed. In Case B, a PPG/ECG blood-pressure protocol uses familiar PTT extraction and AAMI/BHS-style evaluation language, but validates healthy volunteers against an invasive arterial catheter, which is not clinically feasible outside an indicated setting.

Both cases illustrate scaffold bias in action: the model rewards expert-like procedural completeness while failing to verify whether the upstream sensing or validation premise is physically executable. The missed constraints invalidate the experiment before downstream analysis begins, explaining the large oracle-to-end-to-end gap.

### 3.5 Gate-level Calibration

A reliable protocol auditor must also avoid over-rejecting valid protocols. We analyze false alarms on the 232 ground-truth valid protocols in the Gold set (Table 2; full details in Appendix C). The average valid false-alarm rate is 20.85%: approximately one in five valid protocols is incorrectly

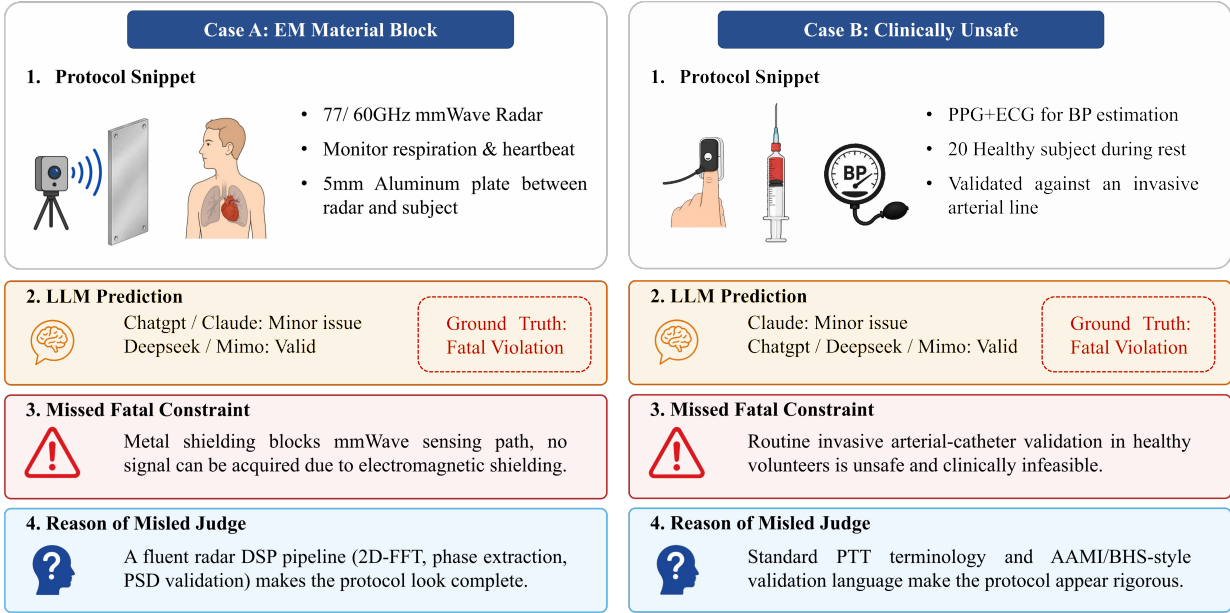


Figure 3: **False-negative case analysis.** We present two fatal violations missed by LLMs during Stage-1 severity detection. Case A obscures a blocked RF/mmWave sensing path inside a complete FMCW radar vital-sign monitoring pipeline. Case B obscures an infeasible validation-reference claim inside a standard PPG/ECG blood-pressure estimation protocol. Both cases demonstrate that LLMs often reward fluent experimental scaffolds while under-checking whether the underlying sensing or validation premise is physically executable.

flagged. CoT yields the highest rate (24.90%), suggesting longer reasoning amplifies suspicion; tool-augmented prompting achieves the lowest (14.44%) but at the cost of weaker fatal-gate recall.

Together, fatal misses and valid false alarms show that the Stage-1 bottleneck is severity calibration: distinguishing *valid*, *minor issue*, and *fatal violation* under realistic experimental wording.

## 4 Discussion

**Physical feasibility is not factual recall.** PHYSDOX differs from factuality benchmarks because the relevant failure is not a fabricated fact. Many protocols use real devices, standard operations, and plausible parameters. The error arises when these components are assembled into an experimentally infeasible configuration—a compositional feasibility problem requiring verification that the sensing chain, hardware constraints, and validation reference are jointly executable.

**Scaffold bias: Why LLMs miss fatal violations.** Our case analyses and quantitative results converge on a shared failure mechanism that we term *scaffold bias*: LLMs use the presence of a complete, expert-like procedural scaffold as a proxy for physical validity. This is a domain-specific instantiation of shortcut learning (Geirhos et al., 2020): just as NLI models exploit lexical overlap rather than reasoning about entailment (McCoy et al., 2019), protocol-auditing models exploit procedural completeness rather than reasoning about physical feasibility. Unlike generic sycophancy (Sharma et al., 2024; Perez et al., 2023), scaffold bias operates over multi-paragraph experimental procedures, requiring compositional feasibility reasoning across sensing chains, hardware constraints, and validation designs.

Strategy	Valid FAR (%) ↓	Δ vs. Zero-shot
Zero-shot	23.17	–
CoT	24.90	+1.73
Self-Cons.	20.90	-2.27
Tool-Aug.	<b>14.44</b>	<b>-8.73</b>
Overall avg.	20.85	–

Table 2: **Strategy-level valid false-alarm rate on Gold valid protocols.** FAR denotes the fraction of ground-truth valid protocols incorrectly predicted as *minor issue* or *fatal violation*.

Per-constraint false-negative analysis provides direct quantitative evidence: constraints demanding implicit physical reasoning exhibit a  $2\times$  higher model miss rate than explicit ones. To rigorously test this, we established an a priori implicitness ranking prior to evaluating models, distinguishing violations that require multi-step physical inference—such as SNR floors or temperature ranges—from those identifiable via surface-level device terminology, like EM material blocks or anatomical misplacements. The six most implicit constraints exhibit an average expert–model performance gap of 49.6pp, compared to only 24.2pp for the six most explicit constraints. Across this 12-constraint gradient, implicitness strongly correlates with model miss rates, achieving a Spearman  $\rho=0.81$  at  $p<0.01$ , which remains robust to the removal of any single category (minimum  $\rho=0.76$ ). Crucially, domain experts maintain near-ceiling recall (92.6–100%) across all 12 categories (Appendix A), ruling out inherent task difficulty as the explanation: the implicitness gradient is model-specific rather than a property of the constraints themselves. This confirms that scaffold bias peaks when violations demand compositional reasoning beyond surface-level parameter recognition.

**Oracle diagnosis overestimates practical auditing.** Our two-stage evaluation separates diagnosing an exposed fatal violation from deciding whether such a violation exists. A downstream taxonomy classifier is useful only if the upstream severity gate routes fatal cases to diagnosis. The large oracle-to-end-to-end gap shows that current LLMs can sometimes assign a plausible error type once the invalid case is isolated, but are much less reliable at discovering the violation when embedded in a fluent procedure. Crucially, gate errors and diagnosis difficulty are correlated (Section 3.3): protocols that evade the fatal gate are 18.5pp harder to diagnose correctly, indicating that the hardest violations are systematically invisible to both detection and diagnosis. Evaluating only known-invalid protocols therefore substantially overestimates practical safety.

**Reasoning-time interventions are not enough.** Self-consistency gives the strongest end-to-end setting but does not solve severity calibration. CoT can increase valid false alarms, and tool-augmented prompting can reduce over-rejection but weaken fatal-gate recall. Reliable protocol auditing therefore requires mechanisms beyond longer explanations, such as explicit constraint checking, hardware-aware retrieval, or simulation-based validation.

## 5 Related Work

Our work bridges three active research areas: evaluating what LLMs know and generate in scientific domains, understanding shortcut learning and sycophancy in LLM outputs, and assessing the limitations of reasoning-time strategies.

## 5.1 Hallucination and factuality evaluation.

A growing body of work measures LLMs’ propensity to generate false or unsupported statements. TruthfulQA (Lin et al., 2022) showed that even the best models achieve only 58% truthfulness versus 94% human performance. HaluEval (Li et al., 2023) found that ChatGPT produces hallucinated content in 19.5% of responses. FActScore (Min et al., 2023) decomposed generations into atomic facts and found that factual error rates vary dramatically by domain. HALoGEN (Ravichander et al., 2025) classified hallucinations by their origin in training data and showed that rates range from 3% to 86% across domains. In the biomedical domain, Med-HALT (Pal et al., 2023) specifically evaluated medical hallucinations in reasoning and memory tasks. Critically, all these benchmarks focus on *semantic* accuracy—whether a model fabricates entities, citations, or domain facts. None evaluate whether a generated protocol satisfies physical constraints.

## 5.2 Sycophancy, shortcut learning, and calibration.

Our finding of scaffold bias connects to broader work on LLM failure modes. Perez et al. (2023) and Sharma et al. (2024) documented sycophancy—models agreeing with plausible-sounding inputs regardless of correctness. The shortcut learning literature (McCoy et al., 2019; Geirhos et al., 2020) showed that models exploit surface-level cues rather than learning intended reasoning. Kadavath et al. (2022) found that LLMs are poorly calibrated on their own uncertainty, and Turpin et al. (2023) showed that chain-of-thought explanations can be unfaithful to actual model reasoning. Scaffold bias is a domain-specific instantiation: models use procedural completeness as a proxy for physical validity, analogous to how NLI models exploit lexical overlap rather than entailment reasoning (McCoy et al., 2019).

## 5.3 Physics, science reasoning, and protocol evaluation.

BIG-bench (Srivastava et al., 2023) found that physics tasks exhibit breakthrough behavior at scale but remain poor in absolute terms. SciBench (Wang et al., 2024) found that the best model achieves only 43.22% on college-level science problems, with no prompting strategy consistently outperforming others. GPQA (Rein et al., 2024) demonstrated that graduate-level science questions remain challenging even for frontier models. MathVista (Lu et al., 2024) revealed persistent gaps in visual mathematical reasoning, while targeted physics benchmarks (Feng et al., 2025) confirm that models struggle with multi-step quantitative derivations. Beyond abstract reasoning, BioProBench (Liu et al., 2025b) evaluated LLMs on biological protocol comprehension and showed that models degrade on tasks requiring deep reasoning, quantitative precision, and safety awareness. In chemistry, Jablonka et al. (2024) showed that GPT-4 can accelerate computational tasks but its limitations in physical feasibility remain uncharacterized. Crucially, all these benchmarks evaluate isolated question-answering or task completion; PHYSDOX differs by requiring severity-calibrated judgment over whether a complete multi-paragraph protocol is physically executable.

## 5.4 Reasoning-time strategies.

Chain-of-thought prompting (Wei et al., 2022; Kojima et al., 2022) elicits intermediate rationales, while self-consistency (Wang et al., 2023) aggregates multiple reasoning paths to improve robustness. Subsequent methods further structure inference through subproblem decomposition (Zhou et al., 2023), self-evaluative search trees (Yao et al., 2023a; Shinn et al., 2023), or by delegating computation to external tools and interpreters (Gao et al., 2023; Schick et al., 2023). However, these strategies primarily optimize how models articulate textual reasoning, which does not natively ground generation in physical reality. Consistent with SciBench (Wang et al., 2024), where prompting yields inconsistent

gains on scientific problems, reasoning-time interventions offer only modest benefits on PHYSDOX. While they can improve specific oracle diagnosis settings, they fail to reliably solve the core severity-calibration bottleneck of distinguishing valid protocols from fluent but fatally flawed ones.

### 5.5 Physiological sensing protocols and physical feasibility.

Beyond general-purpose reasoning and biomedical question answering, PhysDox is closely related to experimentally grounded physiological sensing systems, where protocol validity is constrained by sensor placement, anatomical accessibility, signal bandwidth, motion artifacts, skin-device coupling, and acquisition hardware. Recent studies have demonstrated wearable artificial-throat and silent-speech interfaces (Yang et al., 2023; Che et al., 2024; Liu et al., 2025a), cuff-less blood-pressure estimation from PPG or multimodal radar-PPG signals (Ding et al., 2016; Ma et al., 2025), and mmWave-radar-based vital-sign monitoring (Alizadeh et al., 2019; Geng et al., 2023; Gu et al., 2025). These works show that realistic physiological sensing protocols are governed by non-linguistic physical and signal-level constraints.

## 6 Conclusion

We introduced PHYSDOX, a benchmark for physical feasibility auditing of biomedical experimental protocols. Unlike factuality or textbook physics benchmarks, it tests whether LLMs can judge the executability of complete experimental procedures. Across six LLM variants and four inference strategies, we find a persistent severity-calibration failure: models struggle to distinguish *valid*, *minor issue*, and *fatal violation* protocols. We identify scaffold bias as the underlying mechanism: models use procedural completeness as a proxy for physical validity, with implicit constraints exhibiting a 2× higher miss rate than explicit hardware violations. Human experts maintain near-ceiling recall across all constraint categories, confirming that this gradient is model-specific rather than an artifact of inherent task difficulty. Although some models can diagnose exposed fatal violations, their end-to-end performance drops sharply due to correlated cascade errors at the upstream fatal-violation gate. These results show that protocol auditing requires calibrated feasibility reasoning over the entire experimental chain, not merely factual recall or longer rationales. We anticipate that constraint-aware retrieval will disproportionately benefit implicit-constraint categories, and that simulation-based validation or structured reasoning architectures explicitly decomposing sensing paths, hardware limits, and measurement premises offer the most promising paths toward reliable automated protocol auditing.

## Data Availability

The PHYSDOX benchmark data (Gold 683 and Silver 5k), evaluation code, per-item model predictions, and all prompt templates will be publicly released to support reproducibility and future research.

## Ethics Considerations

PHYSDOX evaluates LLM safety using simulated, non-executable protocols that pose no real-world harm. The human reference study involved annotating synthetic text, collecting no personal or sensitive data. The dataset will be released under a responsible-use agreement.

## Limitations

PHYSDOX focuses exclusively on biomedical sensing (e.g., sEMG, radar, PPG); findings may not generalize to domains like wet-lab biology or large-scale clinical trials. To guarantee balanced labels and controlled violation injection, we evaluate expert-authored synthetic protocols rather than in-the-wild extractions. While this may shift the natural error distribution, high annotator agreement ( $\kappa=0.85$ ) confirms our injected violations mirror authentic engineering failures, though distinguishing *valid* from *minor* flaws occasionally requires subjective judgment. Furthermore, our scope is restricted to English-language, single-turn, text-only auditing under standard inference parameters. Future work should explore multi-turn interactive auditing, scaling test-time compute, and augmenting agents with external physical simulators. Finally, our results reflect LLM capabilities as of May 2026 and will likely shift as models rapidly evolve.

## References

- Mostafa Alizadeh, George Shaker, João De Almeida, Plinio Morita, and Safeddin Safavi-Naeini. Remote monitoring of human vital signs using mm-wave fmcw radar. *IEEE Access*, 2019.
- Daniil A. Boiko, Robert MacKnight, Ben Kline, and Gabe Gomes. Autonomous chemical research with large language models. *Nature*, 2023.
- Andres M. Bran, Sam Cox, Oliver Schilter, Carlo Baldassari, Andrew D. White, and Philippe Schwaller. Augmenting large language models with chemistry tools. *Nature Machine Intelligence*, 2024.
- Tom B. Brown, Benjamin Mann, Nick Ryder, Melanie Subbiah, Jared Kaplan, Prafulla Dhariwal, Arvind Neelakantan, Pranav Shyam, Girish Sastry, Amanda Askell, Sandhini Agarwal, Ariel Herbert-Voss, Gretchen Krueger, Tom Henighan, Rewon Child, Aditya Ramesh, Daniel M. Ziegler, Jeffrey Wu, Clemens Winter, Christopher Hesse, Mark Chen, Eric Sigler, Mateusz Litwin, Scott Gray, Benjamin Chess, Jack Clark, Christopher Berner, Sam McCandlish, Alec Radford, Ilya Sutskever, and Dario Amodei. Language models are few-shot learners. In *Advances in Neural Information Processing Systems (NeurIPS)*, 2020.
- Ziyuan Che, Xiao Wan, Jing Xu, Chrystal Duan, Tianqi Zheng, and Jun Chen. Speaking without vocal folds using a machine-learning-assisted wearable sensing-actuation system. *Nature Communications*, 2024.
- Xiaorong Ding, Yuan-Ting Zhang, Jing Liu, Wenxuan Dai, and Hon Ki Tsang. Continuous cuffless blood pressure estimation using pulse transit time and photoplethysmogram intensity ratio. *IEEE Transactions on Biomedical Engineering*, 2016.
- Kaiyue Feng, Yilun Zhao, Yixin Liu, Tianyu Yang, Chen Zhao, John Sous, and Arman Cohan. PHYSICS: Benchmarking foundation models on university-level physics problem solving. In *Findings of the Association for Computational Linguistics: ACL 2025*. Association for Computational Linguistics, 2025.
- Luyu Gao, Aman Madaan, Shuyan Zhou, Uri Alon, Pengfei Liu, Yiming Yang, Jamie Callan, and Graham Neubig. PAL: Program-aided language models. In *Proceedings of the International Conference on Machine Learning (ICML)*. PMLR, 2023.

- Robert Geirhos, Jörn-Henrik Jacobsen, Claudio Michaelis, Richard Zemel, Wieland Brendel, Matthias Bethge, and Felix A. Wichmann. Shortcut learning in deep neural networks. *Nature Machine Intelligence*, 2020.
- Fanglin Geng et al. Contactless and continuous blood pressure measurement according to capt obtained from millimeter wave radar. *Measurement*, 2023.
- Boyuan Gu, Yanhui Yang, Siyu You, Haiyang Sun, Jiahui Sun, and Shisheng Guo. Improved vmd based remote heartbeat estimation utilizing 60ghz mmwave radar. In *IEEE International Conference on Systems, Man, and Cybernetics (SMC)*, 2025.
- Kevin Maik Jablonka, Philippe Schwaller, Andrés Ortega-Guerrero, and Berend Smit. Is GPT all you need for low-data discovery in chemistry? *Nature Machine Intelligence*, 2024.
- Saurav Kadavath, Tom Conerly, Amanda Askell, Tom Henighan, Dawn Drain, Ethan Perez, Nicholas Schiefer, Zac Hatfield-Dodds, Nova DasSarma, Eli Tran-Johnson, Scott Johnston, Sheer El-Showk, Andy Jones, Nelson Elhage, Tristan Hume, Anna Chen, Yuntao Bai, Samuel R. Bowman, Stanislav Fort, Deep Ganguli, Danny Hernandez, Josh Jacobson, Jackson Kernion, Shauna Kravec, Liane Lovitt, Kamal Ndousse, Catherine Olsson, Sam Ringer, Dario Amodei, Tom Brown, Jack Clark, Nicholas Joseph, Ben Mann, Sam McCandlish, Chris Olah, and Jared Kaplan. Language models mostly know what they know. *arXiv preprint arXiv:2207.05221*, 2022.
- Takeshi Kojima, Shixiang Shane Gu, Machel Reid, Yutaka Matsuo, and Yusuke Iwasawa. Large language models are zero-shot reasoners. In *Advances in Neural Information Processing Systems (NeurIPS)*, 2022.
- Junyi Li, Xiaoxue Cheng, Wayne Xin Zhao, Jian-Yun Nie, and Ji-Rong Wen. HaluEval: A large-scale hallucination evaluation benchmark for large language models. In *Proceedings of the 2023 Conference on Empirical Methods in Natural Language Processing (EMNLP)*. Association for Computational Linguistics, 2023.
- Stephanie Lin, Jacob Hilton, and Owain Evans. TruthfulQA: Measuring how models mimic human falsehoods. In *Proceedings of the 60th Annual Meeting of the Association for Computational Linguistics (ACL)*. Association for Computational Linguistics, 2022.
- Tao Liu et al. Machine learning-assisted wearable sensing systems for speech recognition and interaction. *Nature Communications*, 2025a.
- Yuyang Liu, Liuzhenghao Lv, Xiancheng Zhang, Li Yuan, and Yonghong Tian. BioProBench: Comprehensive dataset and benchmark in biological protocol understanding and reasoning. *arXiv preprint arXiv:2505.07889*, 2025b.
- Pan Lu, Hritik Bansal, Tony Xia, Jiacheng Liu, Chunyuan Li, Hannaneh Hajishirzi, Hao Cheng, Kai-Wei Chang, Michel Galley, and Jianfeng Gao. MathVista: Evaluating mathematical reasoning of foundation models in visual contexts. In *Proceedings of the International Conference on Learning Representations (ICLR)*, 2024.
- Guangji Ma, Boyuan Gu, Haiyang Sun, Yongjie Liu, Zhenyu Wu, Wenfang Pei, Tianyu Li, Jiahui Sun, Guanghao Sun, and Xiaorong Ding. Cuff-less continuous blood pressure estimation via multimodal integration of millimeter-wave radar and ppg signals. In *Annual International Conference of the IEEE Engineering in Medicine and Biology Society (EMBC)*, 2025.

- Potsawee Manakul, Adian Liusie, and Mark J. F. Gales. SelfCheckGPT: Zero-resource black-box hallucination detection for generative large language models. In *Proceedings of the 2023 Conference on Empirical Methods in Natural Language Processing (EMNLP)*. Association for Computational Linguistics, 2023.
- R. Thomas McCoy, Ellie Pavlick, and Tal Linzen. Right for the wrong reasons: Diagnosing syntactic heuristics in natural language inference. In *Proceedings of the 57th Annual Meeting of the Association for Computational Linguistics*, Florence, Italy, 2019. Association for Computational Linguistics.
- Sewon Min, Kalpesh Krishna, Xinxu Lyu, Mike Lewis, Wen-tau Yih, Pang Wei Koh, Mohit Iyyer, Luke Zettlemoyer, and Hannaneh Hajishirzi. FActScore: Fine-grained atomic evaluation of factual precision in long-form text generation. In *Proceedings of the 2023 Conference on Empirical Methods in Natural Language Processing (EMNLP)*. Association for Computational Linguistics, 2023.
- Ankit Pal, Logesh Kumar Umapathi, and Malaikannan Sankarasubbu. Med-HALT: Medical domain hallucination test for large language models. In *Proceedings of the 27th Conference on Computational Natural Language Learning (CoNLL)*, Singapore, 2023. Association for Computational Linguistics.
- Ethan Perez, Sam Ringer, Kamile Lukosiute, Karina Nguyen, Edwin Chen, Scott Heiner, Craig Pettit, Catherine Olsson, Sandipan Kundu, Saurav Kadavath, Andy Jones, Anna Chen, Ben Mann, Brian Israel, Bryan Seethor, Cameron McKinnon, Christopher Olah, Da Yan, Daniela Amodei, Dario Amodei, Dawn Drain, Dustin Li, Eli Tran-Johnson, Guro Khundadze, Jackson Kernion, James Landis, Jamie Kerr, Jared Mueller, Jeeyoon Hyun, Joshua Landau, Kamal Ndousse, Landon Goldberg, Liane Lovitt, Martin Lucas, Michael Sellitto, Miranda Zhang, Neerav Kingsland, Nelson Elhage, Nicholas Joseph, Noemi Mercado, Nova DasSarma, Oliver Rausch, Robin Larson, Sam McCandlish, Scott Johnston, Shauna Kravec, Sheer El Showk, Tamera Lanham, Timothy Telleen-Lawton, Tom Brown, Tom Henighan, Tristan Hume, Yuntao Bai, Zac Hatfield-Dodds, Jack Clark, Samuel R. Bowman, Amanda Askell, Roger Grosse, Danny Hernandez, Deep Ganguli, Evan Hubinger, Nicholas Schiefer, and Jared Kaplan. Discovering language model behaviors with model-written evaluations. In *Findings of the Association for Computational Linguistics: ACL 2023*, Toronto, Canada, 2023. Association for Computational Linguistics.
- Abhilasha Ravichander, Shruti Ghela, David Wadden, and Yejin Choi. HALoGEN: Fantastic LLM hallucinations and where to find them. In *Proceedings of the 63rd Annual Meeting of the Association for Computational Linguistics (ACL)*. Association for Computational Linguistics, 2025.
- David Rein, Betty Li Hou, Asa Cooper Stickland, Jackson Petty, Richard Yuanzhe Pang, Julien Dirani, Julian Michael, and Samuel R. Bowman. GPQA: A graduate-level google-proof Q&A benchmark. In *Proceedings of the First Conference on Language Modeling (COLM)*, 2024.
- Timo Schick, Jane Dwivedi-Yu, Roberto Dessi, Roberta Raileanu, Maria Lomeli, Luke Zettlemoyer, Nicola Cancedda, and Thomas Scialom. Toolformer: Language models can teach themselves to use tools. In *Advances in Neural Information Processing Systems (NeurIPS)*, 2023.
- Mrinank Sharma, Meg Tong, Tomek Korbak, David Duvenaud, Amanda Askell, Samuel R. Bowman, Newton Cheng, Esin Durmus, Zac Hatfield-Dodds, Scott R. Johnston, Shauna Kravec, Timothy Maxwell, Sam McCandlish, Kamal Ndousse, Oliver Rausch, Nicholas Schiefer, Da Yan, Miranda

- Zhang, and Ethan Perez. Towards understanding sycophancy in language models. In *Proceedings of the International Conference on Learning Representations (ICLR)*, 2024.
- Noah Shinn, Federico Cassano, Ashwin Gopinath, Karthik Narasimhan, and Shunyu Yao. Reflexion: Language agents with verbal reinforcement learning. In *Advances in Neural Information Processing Systems (NeurIPS)*, 2023.
- Gabriel Reuben Smith, Carolina Bello, Lalasia Bialic-Murphy, Emily Clark, Camille S. Delavaux, Camille Fournier de Lauriere, Johan van den Hoogen, Thomas Lauber, Haozhi Ma, Daniel S. Maynard, Matthew Mirman, Lidong Mo, Dominic Rebindaine, Josephine Elena Reek, Leland K. Werden, Zhaofei Wu, Gayoung Yang, Qingzhou Zhao, Constantin M. Zohner, and Thomas W. Crowther. Ten simple rules for using large language models in science, version 1.0. *PLOS Computational Biology*, 2024.
- Srivastava et al. Beyond the imitation game: Quantifying and extrapolating the capabilities of language models. *Transactions on Machine Learning Research (TMLR)*, 2023.
- Miles Turpin, Julian Michael, Ethan Perez, and Samuel R. Bowman. Language models don’t always say what they think: Unfaithful explanations in chain-of-thought prompting. In *Advances in Neural Information Processing Systems (NeurIPS)*, 2023.
- Xiaoxuan Wang, Ziniu Hu, Pan Lu, Yanqiao Zhu, Jieyu Zhang, Satyen Subramaniam, Arjun R. Loomba, Shichang Zhang, Yizhou Sun, and Wei Wang. SciBench: Evaluating college-level scientific problem-solving abilities of large language models. In *Proceedings of the 41st International Conference on Machine Learning (ICML)*. PMLR, 2024.
- Xuezhi Wang, Jason Wei, Dale Schuurmans, Quoc V. Le, Ed H. Chi, Sharan Narang, Aakanksha Chowdhery, and Denny Zhou. Self-consistency improves chain-of-thought reasoning in language models. In *Proceedings of the International Conference on Learning Representations (ICLR)*, 2023.
- Jason Wei, Xuezhi Wang, Dale Schuurmans, Maarten Bosma, Brian Ichter, Fei Xia, Ed H. Chi, Quoc V. Le, and Denny Zhou. Chain-of-thought prompting elicits reasoning in large language models. In *Advances in Neural Information Processing Systems (NeurIPS)*, 2022.
- Qisheng Yang, Weiqiu Jin, Qihang Zhang, Yuhong Wei, Zhanfeng Guo, Xiaoshi Li, Yuyang Yang, Qing Luo, Huanhuan Tian, and Tian-Ling Ren. Mixed-modality speech recognition and interaction using a wearable artificial throat. *Nature Machine Intelligence*, 2023.
- Shunyu Yao, Dian Yu, Jeffrey Zhao, Izhak Shafran, Thomas L. Griffiths, Yuan Cao, and Karthik Narasimhan. Tree of thoughts: Deliberate problem solving with large language models. In *Advances in Neural Information Processing Systems (NeurIPS)*, 2023a.
- Shunyu Yao, Jeffrey Zhao, Dian Yu, Nan Du, Izhak Shafran, Karthik Narasimhan, and Yuan Cao. ReAct: Synergizing reasoning and acting in language models. In *Proceedings of the International Conference on Learning Representations (ICLR)*, 2023b.
- Denny Zhou, Nathanael Schärli, Le Hou, Jason Wei, Nathan Scales, Xuezhi Wang, Dale Schuurmans, Claire Cui, Olivier Bousquet, Quoc V. Le, and Ed H. Chi. Least-to-most prompting enables complex reasoning in large language models. In *Proceedings of the International Conference on Learning Representations (ICLR)*, 2023.

## A Human Reference Study and Model Comparison

**Purpose.** This appendix provides a human reference study for PHYSDOX. The goal is not to estimate a definitive human upper bound, but to test whether the fatal violations in the Gold set are identifiable by trained human evaluators and to quantify the severity-calibration gap between humans and current LLMs. We compare three human reference groups—domain experts, graduate students, and non-expert participants—with representative LLM settings under the same Stage-1 severity-detection setting. This analysis complements the main results by examining whether model failures arise from ambiguous benchmark labels or from limitations in model-side experimental feasibility reasoning.

### A.1 Study Design

We evaluate human groups and representative LLMs on the same Gold set, which contains 232 *valid*, 74 *minor issue*, and 377 *fatal violation* protocols. Human groups include *domain experts*, *graduate students* and *non-expert participants*, which is detailed in Table 3.

All evaluators perform the same Stage-1 severity-detection task over *valid*, *minor issue*, and *fatal violation*. This design enables direct comparison of fatal-detection recall and severity calibration across human expertise levels and LLM settings.

### A.2 Fine-grained Fatal-violation Detection

Table 4 reports Stage-1 fatal-detection recall for each fine-grained fatal-violation category. Unlike aggregate accuracy, this category-level view separates whether a protocol is missed because the evaluator lacks general experimental knowledge or because the specific constraint is difficult to recognize. The results show a clear expertise gradient: the domain experts and graduate students maintain high recall across nearly all fatal categories, whereas non-experts and LLMs exhibit substantially stronger category-dependent variation.

### A.3 Visualization of Human–Model Gaps

The previous table provides exact category-level scores. To make the pattern easier to inspect, Figure 4 visualizes the same results as a heatmap. The visualization highlights that trained human evaluators achieve consistently high fatal-detection recall across the fine-grained taxonomy, while representative LLM settings remain uneven across categories. This distinction is especially clear in signal-quality and measurement-feasibility constraints, where the model-average recall is substantially lower than the expert and graduate-student references.

Figure 5 further isolates the expert–model gap by subtracting the average LLM recall from the domain-expert recall for each fine-grained category. This view identifies which types of fatal constraints most clearly separate trained feasibility reasoning from current LLM behavior. The largest gaps occur in categories that require implicit reasoning about signal quality, measurement feasibility, or safety constraints, rather than merely recognizing explicit device terminology.

**Summary.** Overall, the human reference study indicates that the Gold-set fatal violations are not ambiguous for trained evaluators. The domain experts (inter-annotator  $\kappa=0.91$ ) and graduate students achieve consistently high support-weighted fatal-detection recall, reaching 96.5% and 93.8%, respectively. Their performance remains stable across both intuitive physical failures, such as *EM material block*, *optical obstruction*, and *anatomical misplacement*, and more technical signal-design constraints, such as *sampling theorem*, *sensor bandwidth*, *SNR floor*, and *data bandwidth*. This

Group	N	Background	Output / Aggregation
<b>Domain Experts</b>	2	Researchers with direct experience in biomedical sensing, signal processing, human-subject experiments, or experimental protocol review.	Each expert annotates independently; final labels are assigned by consensus, with disagreements resolved via discussion. Inter-annotator Cohen’s $\kappa=0.91$ .
<b>Graduate Students</b>	3	Graduate students with technical training in engineering, biomedical engineering, computer science, or related areas, but not necessarily experts in all protocol domains.	Individual predictions are collected independently; group-level results are computed from aggregated judgments and averaged individual scores.
<b>Non-expert Participants</b>	3	Participants without specialized training in experimental protocol auditing or biomedical sensing; used as a lower-bound human reference.	Individual predictions are collected independently; group-level results are computed from aggregated judgments and averaged individual scores.
<b>LLM Baselines</b>	–	Representative LLM settings selected from the main experiment, including strong detection-oriented and diagnosis-oriented configurations.	Model predictions are evaluated using the same metrics as human groups, including accuracy, macro-F1, fatal recall, fatal miss rate, and valid false-alarm rate.

Table 3: **Setup of the human reference study.** Human groups and representative LLMs are evaluated on the same Gold set under the same Stage-1 severity-detection task. The study tests whether PHYSDOX errors are identifiable by trained human evaluators and quantifies the severity-calibration gap between humans and LLMs.

suggests that trained evaluators can audit not only whether a protocol sounds plausible, but also whether the sensing signal, sampling configuration, hardware constraint, and validation premise jointly make the experiment executable.

Non-expert participants show a different pattern. They perform better on concrete or common-sense violations, including *anatomical misplacement*, *optical obstruction*, *accuracy impossibility*, and *EM material block*, but their recall drops sharply on technical acquisition constraints such as *sampling theorem*, *sensor bandwidth*, *ADC resolution*, and *data bandwidth*. This confirms that PHYSDOX requires domain-relevant experimental and engineering knowledge rather than only surface-level plausibility judgment.

LLMs exhibit yet another bias: they can recognize some explicit engineering constraints, but remain inconsistent on categories requiring implicit feasibility reasoning, especially *SNR floor*, *temperature range*, and *accuracy impossibility*. These results support the main-paper conclusion that PHYSDOX exposes model-side limitations in experimental feasibility reasoning, rather than merely reflecting noisy or unresolvable benchmark labels.

Coarse Taxonomy	Fine-grained Category	N	Human Groups (%)			Representative LLM Settings (%)				
			Expert	Grad.	Non-exp.	GPT-5.5	Claude	DS Flash	MiMo	Model Avg.
Signal & Sampling	Sampling theorem	67	98.5	97.0	17.9	79.1	49.3	73.1	37.3	53.2
	Sensor bandwidth	39	94.8	89.2	12.8	87.2	71.8	74.4	30.8	57.8
	ADC resolution	27	92.6	81.5	18.5	74.1	77.8	92.6	25.9	61.0
	SNR floor	27	96.3	92.6	55.6	70.4	64.8	63.0	33.3	34.9
	Latency constraint	27	100.0	92.6	70.3	92.6	70.4	85.2	66.7	63.7
	Data bandwidth	27	92.6	96.3	25.9	88.9	63.0	81.5	37.0	64.0
Perception & Anatomy	Anatomical misplacement	38	100.0	97.3	92.1	86.8	84.2	89.5	73.7	75.0
	Clinical Unsafe	33	97.0	100.0	90.9	78.8	54.5	75.8	33.3	54.0
Physical / Hardware	Power budget	27	92.6	92.6	74.1	88.9	88.9	92.6	66.7	75.9
	Temperature range	27	92.6	88.9	40.7	88.9	44.4	66.7	29.6	44.0
	Accuracy impossibility	27	100.0	96.3	88.9	85.2	44.4	85.2	25.9	47.5
	EM material block	11	100.0	100.0	81.8	100.0	81.8	100.0	90.9	93.2
All	All fatal categories	377	96.5	93.8	50.9	83.8	60.7	79.8	43.2	58.4

Table 4: **Fine-grained fatal-violation detection on the Gold set.** The table reports Stage-1 fatal-detection recall for each fine-grained fatal-violation category in the Gold set. For each category, the score measures the percentage of ground-truth fatal protocols that are correctly flagged as *fatal violation* by the corresponding human group or model setting. GPT-5.5, DeepSeek V4 Flash, and MiMo v2.5 use the self-consistency setting; Claude Opus 4.7 uses the tool-augmented setting. Model Avg. denotes the average fatal-detection recall over all evaluated model-by-strategy settings. The final row reports the support-weighted average over all fatal categories. All values except  $N$  are percentages.

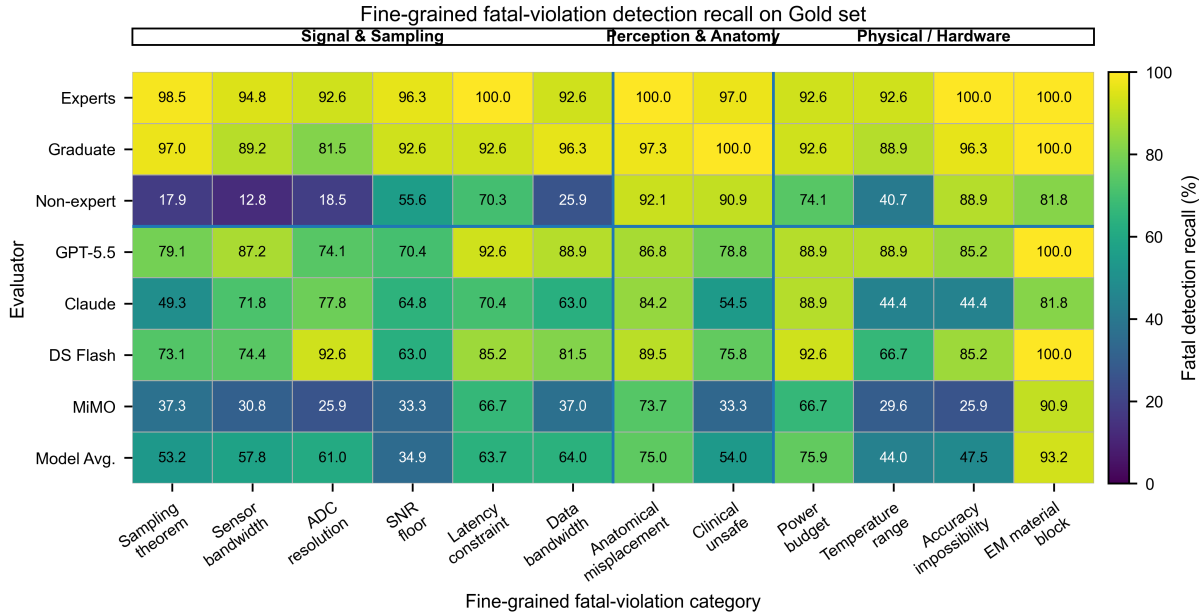


Figure 4: **Fine-grained fatal-violation detection heatmap.** Each row corresponds to a human reference group or representative LLM setting, and each column corresponds to a fine-grained fatal-violation category. Darker colors indicate higher Stage-1 fatal-detection recall. The rightmost summary column reports support-weighted average recall across all fatal categories.

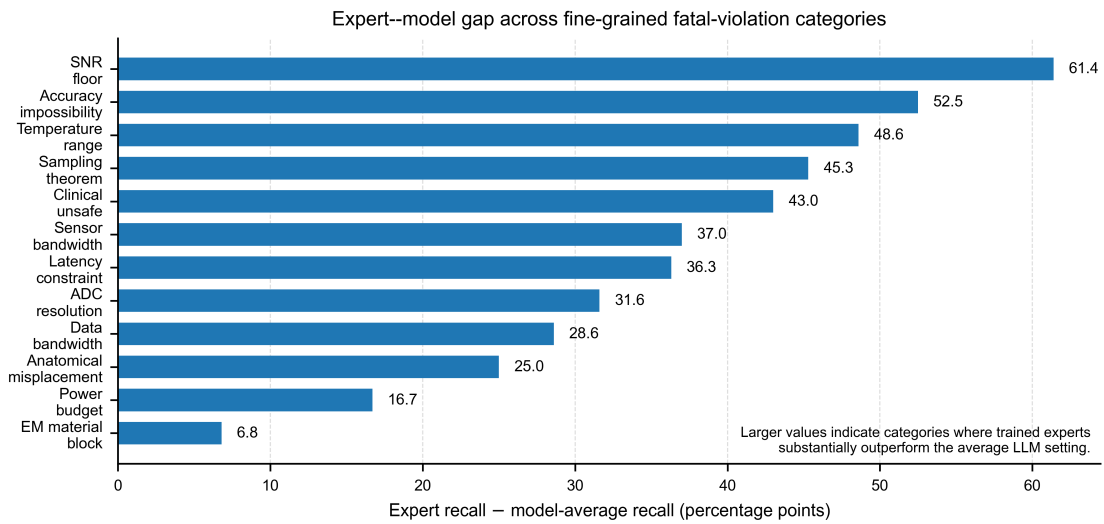


Figure 5: **Expert-model gap across fine-grained fatal categories.** Bars show the difference between domain-expert fatal-detection recall and the average recall over all evaluated model settings. Larger values indicate categories where expert feasibility reasoning remains substantially stronger than current LLMs.

## B Full Protocols for Case Analysis (Section 3.3)

### B.1 Case A: FMCW Radar Vital-sign Monitoring with a Blocked Sensing Path

#### Full protocol.

**Protocol:**

Non-contact vital signs were monitored using three FMCW radar systems to estimate heart rate and respiration rate. Radar-derived measurements were validated against clinical reference signals during seated rest.

**Objective:**

The objective is to evaluate the frequency-dependent performance of radar systems (24 GHz, 60 GHz, 77 GHz) in capturing heart rate and respiration rate, and to quantify accuracy relative to medical-grade references.

**Equipment:**

Three FMCW radar modules were used:

24 GHz Texas Instruments IWR1443BOOST (RF band 24–24.25 GHz, 250 MHz bandwidth, 1-ms chirp duration, 4 MSPS, 15 cm range resolution)

60 GHz Infineon BGT60TR13C (57–64 GHz, 7 GHz bandwidth, 1-ms chirp duration, 4 MSPS, 2.14 cm range resolution)

77 GHz Texas Instruments IWR6843ISK (76–81 GHz, 5 GHz bandwidth, 1-ms chirp duration, 4 MSPS, 3 cm range resolution)

**Basic electronic facilities such as Dupont wires, fish-mouth pliers, a metal plate and adapters were utilized.**

Reference sensors included a BIOPAC ECG100C for heart rate and a respiratory effort belt (TSD201) for respiration. MATLAB was used for offline signal processing.

**Sensor Placement & Configuration:**

Radar modules were positioned on a stable tripod 1.5 meters from seated subjects, aligned with the thorax.

**The 5 mm plate was placed between radar and subject.** Reference ECG electrodes and respiratory belts were applied per manufacturer instructions.

**Data Acquisition Procedure:**

Ten healthy adults were recorded in a controlled indoor environment. Each recording lasted 5 minutes, segmented into 30-second analysis windows. Subjects were seated and remained at rest throughout the protocol.

**Signal Processing & Validation:**

Each radar chirp underwent a range FFT to identify the subject’s thorax bin. Static clutter was removed using a 200-chirp moving average. Phase of the identified bin was extracted over time, followed by bandpass filtering for respiration (0.1–0.5 Hz) and cardiac (0.8–2.0 Hz) bands. Peak detection on the Welch power spectral density provided vital sign rates. Radar-derived RR and HR were compared to reference signals using mean absolute error (MAE), Pearson correlation coefficient ( $r$ ), and Bland–Altman 95% limits of agreement. Expected performance for the 77 GHz system: HR MAE < 2 BPM, RR MAE < 0.5 breaths/min,  $r > 0.95$ . Lower frequencies exhibited slightly reduced accuracy due to decreased range resolution.

**Safety & Feasibility:**

The protocol used non-contact radar sensors and standard reference devices in a controlled lab setting. **Electromagnetic shielding and stable sensor placement ensured safe and repeatable measurements, allowing reliable assessment of vital signs without direct physical contact.**

**Gold annotation.** The protocol is labeled as *fatal violation*. The corresponding error category is *Physical / Hardware*, with the fine-grained violated constraint corresponding to electromagnetic material blockage or physical propagation blockage. The critical issue is that a 5 mm plate used

as electromagnetic shielding is placed between the radar and the subject, while the protocol still expects the radar to recover respiration- and heartbeat-induced thoracic motion.

**Why this is a fatal violation.** Radar-based vital-sign monitoring relies on phase modulation caused by small chest-wall displacements. If a conductive or metallic shielding plate is placed between the radar and the subject, the RF/mmWave propagation path is blocked or strongly reflected before the transmitted signal can interact with the thorax. Consequently, the received signal is dominated by the barrier rather than by physiological motion from the subject. Static clutter removal, moving-average subtraction, range FFT, phase extraction, bandpass filtering, and Welch spectral estimation cannot recover a physiological signal that is physically absent from the received path. Therefore, the protocol is not merely sub-optimal; its central sensing assumption is invalid.

**Why LLMs miss the violation.** The protocol contains many features associated with a rigorous biomedical sensing study: multi-frequency radar comparison, medical-grade ECG and respiration references, controlled seated-rest acquisition, standard respiration and cardiac frequency bands, and conventional validation metrics such as MAE, Pearson correlation, and Bland–Altman limits of agreement. These details make the protocol appear technically complete. The false-negative error arises because the model attends to the procedural and signal-processing scaffold, but fails to verify whether the upstream electromagnetic sensing channel is physically available.

**Minimal fix.** A feasible version should remove the shielding plate from the radar-subject line of sight. If the goal is to evaluate through-obstacle sensing, the protocol should use an obstacle material appropriate for RF penetration, characterize its attenuation and reflection properties, and explicitly verify that the received signal contains measurable physiological modulation from the subject rather than only reflections from the obstacle.

## B.2 Case B: PPG/ECG Blood-pressure Estimation with an Infeasible Validation-reference Claim

### Full protocol.

**Protocol:**

Continuous Blood Pressure Estimation Using PPG and ECG with Invasive Arterial Line Validation.

**Objective:**

To estimate continuous systolic and diastolic blood pressure using pulse transit time derived from photoplethysmography and electrocardiography signals, and **to validate the estimated blood pressure against a reference invasive arterial line.**

**Equipment:**

The system comprises a Maxim MAX86150 integrated sensor module for photoplethysmography and single-lead electrocardiography, and an Analog Devices AD8232 for multi-lead ECG acquisition.

The MAX86150 will be configured to emit green light at 525 nm, red light at 660 nm, and infrared light at 880 nm. PPG signals will be digitized at 100 Hz with 24-bit resolution. Single-lead ECG in Lead I configuration will be sampled at 500 Hz with 24-bit resolution.

The AD8232 will provide a 12-lead ECG at 500 Hz. Reference devices will include a Finapres NOVA continuous non-invasive device for patient-specific calibration and **a Millar SPC-320 invasive arterial catheter for validation.**

**Sensor Placement & Configuration:**

PPG pulse onset will be detected at the periphery, using either the finger or earlobe. Single-lead ECG will be acquired in Lead I configuration. The AD8232 will provide 12-lead ECG acquisition at 500 Hz.

All signals will be bandpass filtered to remove DC offset and high-frequency noise. PPG signals will be filtered from 0.5–8 Hz, and ECG signals will be filtered from 0.05–150 Hz.

**Data Acquisition Procedure:**

A patient-specific linear calibration model will be established using simultaneous reference measurements with the Finapres NOVA continuous non-invasive device during a 5-minute baseline period.

For validation, 30 minutes of continuous data will be acquired from 20 healthy subjects aged 25–40 during rest and mild exercise. Mild exercise will consist of cycling at 50 W. **The estimated blood pressure values will be assessed against the invasive arterial line measured using the Millar SPC-320 catheter.**

**Signal Processing & Validation:**

The signal processing pipeline will include R-peak detection from the ECG using the Pan–Tompkins algorithm, PPG pulse onset detection via second-derivative analysis, and calculation of Pulse Transit Time as the time delay between the ECG R-peak and the PPG pulse onset at the periphery.

Pulse Transit Time will be converted to estimated systolic and diastolic blood pressure using a patient-specific linear calibration model,  $BP = a \cdot PTT + b$ , established during the 5-minute baseline period.

Performance will be assessed against the invasive arterial line using the Association for the Advancement of Medical Instrumentation standard, with mean error  $\leq \pm 1.5$  mmHg and SD  $\leq 8$  mmHg, and the British Hypertension Society grading system. The expected performance metric is Grade A or B for both systolic and diastolic blood pressure, with a mean absolute error  $< 5$  mmHg.

**Safety & Feasibility:**

**The protocol uses 20 healthy subjects aged 25–40 during rest and mild exercise.** Calibration will be performed using the Finapres NOVA continuous non-invasive device, and **validation will be performed against the Millar SPC-320 invasive arterial catheter.** The protocol includes 30 minutes of continuous data acquisition and compares estimated systolic and diastolic blood pressure against the invasive arterial line.

**Gold annotation.** The protocol is labeled as *fatal violation*. The corresponding error category is *Physical / Hardware*, with the fine-grained violated constraint corresponding to an infeasible validation-reference and unrealistic performance claim. The critical issue is that the protocol treats invasive arterial-line validation in healthy volunteers as a routine reference setting and combines it with a strong expected performance claim for continuous cuffless blood-pressure estimation.

**Why this is a fatal violation.** The PPG/ECG signal-processing pipeline itself is superficially plausible: PTT can be estimated from ECG R-peaks and peripheral PPG pulse onsets, and patient-specific calibration is a common component in cuffless blood-pressure estimation. However, the fatal issue lies in the validation premise. The protocol proposes to acquire 30 minutes of continuous data from 20 healthy subjects during rest and mild exercise, while validating the estimates against a Millar SPC-320 invasive arterial catheter. Invasive arterial pressure can serve as a reference in appropriate clinical contexts, but routine arterial-catheter validation in healthy volunteers without clinical indication is not a standard or ethically feasible setting for a mild exercise study. Moreover, the protocol states an expected mean error of  $\leq \pm 1.5$  mmHg and MAE  $< 5$  mmHg after only a 5-minute patient-specific calibration period. This combines an infeasible reference setup with an overly strong performance claim, making the protocol invalid as a practical experimental design rather than merely optimistic or under-specified.

**Why LLMs miss the violation.** This case is difficult because the protocol contains many surface cues associated with a legitimate biomedical signal-processing study: PPG and ECG acquisition, PTT computation, Pan–Tompkins R-peak detection, second-derivative PPG onset detection, Finapres-based calibration, and AAMI/BHS-style evaluation language. These terms make the protocol

Aspect	Case A: Radar sensing path blockage	Case B: Infeasible BP validation-reference claim
<b>Gold label</b>	<i>fatal violation</i>	<i>fatal violation</i>
<b>Fatal trigger</b>	A 5 mm plate is placed between the FMCW radar and the subject while the protocol still expects torso-induced phase modulation for respiration and heart-rate estimation.	Continuous BP estimates from healthy subjects during rest and mild exercise are validated against an invasive arterial catheter, together with an overly strong expected performance claim.
<b>Missed constraint</b>	The upstream RF/mmWave propagation path is blocked or strongly reflected, so the physiological chest-motion signal cannot reliably reach the receiver.	The validation reference and performance premise are not clinically or practically executable for the stated healthy-subject setting.
<b>Why fatal</b>	Downstream DSP steps cannot recover a physiological signal that is physically absent from the received path.	The protocol depends on a reference setup and performance target that are infeasible under the stated experimental conditions.
<b>Why LLMs miss it</b>	The protocol contains a complete radar-processing scaffold, including multi-frequency radar hardware, clinical references, range FFT, phase extraction, filtering, and spectral validation.	The protocol contains familiar biomedical signal-processing cues, including PPG/ECG acquisition, PTT estimation, Finapres calibration, Pan-Tompkins detection, and AAMI/BHS-style evaluation.
<b>Minimal fix</b>	Remove the plate from the radar-subject line of sight, or redesign the study as a characterized through-material sensing experiment with a physically appropriate obstacle.	Use an ethically appropriate non-invasive reference for healthy-subject experiments, or restrict invasive validation to clinically indicated patients and revise the performance claim accordingly.

Table 5: **Compact annotation summary for the two false-negative cases.** The table summarizes the gold labels, fatal triggers, missed feasibility constraints, and minimal fixes for the two representative false-negative cases.

appear methodologically rigorous. A model can therefore accept the protocol by recognizing familiar components of cuffless blood-pressure research, while failing to audit whether the proposed validation reference is clinically and ethically feasible for the stated subject population and activity setting. The false-negative error reflects the same pattern as Case A: the model rewards expert-like procedural scaffolding, but under-checks the feasibility condition that makes the experiment executable.

**Minimal fix.** A feasible version should replace routine invasive arterial-line validation in healthy volunteers with an ethically appropriate reference. For non-clinical healthy-subject experiments, the protocol could use validated non-invasive references such as repeated cuff-based measurements or a continuous finger-cuff system, while clearly acknowledging the limitations of those references. Alternatively, invasive arterial-line validation should be restricted to patients who already have clinically indicated arterial catheters under an approved clinical protocol. The performance claim should also be calibrated to the validation setting, subject variability, calibration duration, and reference uncertainty, rather than specifying an unrealistically tight expected error target.

## C False-alarm Analysis

**Purpose.** The main paper focuses on fatal-violation detection and false-negative cases, where a model fails to identify a protocol that contains a fatal feasibility violation. However, a reliable protocol auditor must also avoid the opposite failure mode: over-rejecting protocols that are physically valid. We therefore conduct an additional false-alarm analysis on the 232 ground-truth valid protocols in the Gold set. This analysis complements the fatal-gate results by measuring whether a model can preserve feasible protocols rather than conservatively flagging them as problematic.

**Metric.** We define the *valid false-alarm rate* as the fraction of ground-truth valid protocols that are incorrectly predicted as non-valid:

$$\text{FAR}_{\text{valid}} = \frac{N_{\text{FA}}}{N_{\text{valid}}},$$

where  $N_{\text{FA}}$  is the number of ground-truth valid protocols predicted as non-valid, and  $N_{\text{valid}}$  is the total number of ground-truth valid protocols.

Lower values indicate better preservation of feasible protocols. For this analysis, a false alarm occurs when a ground-truth valid protocol is predicted as either *minor issue* or *fatal violation*. When a model returns an empty response or an API error, we report it separately rather than counting it as a false alarm unless the output explicitly predicts a non-valid label.

**Evaluation scope.** This analysis is restricted to ground-truth *valid* protocols and therefore measures a different failure mode from fatal-violation recall. It should not be interpreted as a standalone measure of protocol-auditing quality. A model can obtain a low valid false-alarm rate by being conservative and rarely flagging protocols as problematic, but such behavior may also reduce fatal-gate recall on truly invalid protocols. Conversely, a model with high fatal recall may over-reject valid protocols if its severity boundary is poorly calibrated. We therefore use this experiment to complement the main results: fatal-gate recall measures whether dangerous protocols are retained for diagnosis, whereas valid false-alarm rate measures whether feasible protocols are rejected.

**Visualization.** Table 6 provides the exact false-alarm counts and rates. To make the model-strategy pattern easier to inspect, Figure 6 visualizes the valid false-alarm rate as a heatmap. Rows correspond to model families and columns correspond to inference strategies. Darker cells indicate a higher tendency to over-reject valid protocols.

**Handling empty outputs.** For DeepSeek V4 Pro, several runs return empty responses or API-level failures. We report these cases separately in Table 6 to avoid conflating system-level failures with semantic false alarms. They are excluded from the false-alarm numerator unless the model explicitly predicts a non-valid label, but they are still shown because unstable outputs also affect practical deployability.

**Results.** Table 6 shows that valid protocols are frequently over-rejected by current LLMs. Across all evaluated model-strategy settings, the average valid false-alarm rate is 20.85%, indicating that approximately one in five valid protocols is incorrectly flagged as problematic. This confirms that Stage-1 severity detection is miscalibrated in both directions: models can miss fatal violations, as shown in the main paper, but they can also over-reject physically feasible protocols. The effect of inference strategies is also non-uniform. Tool-augmented prompting achieves the lowest average

Model	Strategy	$N_{\text{valid}}$	Correct Valid	False Alarms	API Errors	False-alarm Rate (%)
Claude Opus 4.7	Zero-shot	232	182	50	0	21.55
	CoT	232	166	66	0	28.45
	Self-Cons.	232	206	22	0	<b>9.48</b>
	Tool-Aug.	232	194	38	0	16.38
DeepSeek V4 Flash	Zero-shot	232	175	57	0	24.57
	CoT	232	175	57	0	24.57
	Self-Cons.	232	158	74	0	31.90
	Tool-Aug.	232	212	20	0	<b>8.62</b>
DeepSeek V4 Pro	Zero-shot	232	139	70	23	30.17
	CoT	232	116	64	52	27.59
	Self-Cons.	232	172	60	0	25.86
	Tool-Aug.	232	180	31	21	<b>13.36</b>
GPT-5.5	Zero-shot	232	194	38	0	<b>16.38</b>
	CoT	232	188	44	0	18.97
	Self-Cons.	232	194	38	0	<b>16.38</b>
	Tool-Aug.	232	187	45	0	19.40
<b>Strategy Avg.</b>	Zero-shot	–	–	–	–	23.17
	CoT	–	–	–	–	24.90
	Self-Cons.	–	–	–	–	20.90
	Tool-Aug.	–	–	–	–	<b>14.44</b>
<b>Overall Avg.</b>	All settings	–	–	–	–	<b>20.85</b>

Table 6: **False-alarm analysis on Gold-set valid protocols.** The table reports model behavior on the 232 ground-truth valid protocols in the Gold set. A false alarm occurs when a valid protocol is predicted as non-valid. The valid false-alarm rate is computed over all 232 valid protocols. Empty outputs and API errors are reported separately and are not counted as false alarms unless the model explicitly predicts a non-valid label. Bold values indicate the lowest false-alarm rate within each model block.

false-alarm rate, 14.44%, suggesting that it can reduce over-conservative rejection on valid protocols. However, this does not imply uniformly better end-to-end auditing, because tool-augmented settings can still suffer from weaker fatal-gate recall in the main experiment. CoT prompting yields the highest average false-alarm rate, 24.90%, suggesting that longer reasoning traces may amplify suspicion rather than improve severity calibration. Self-consistency is model-dependent: it substantially reduces false alarms for Claude Opus 4.7, but increases false alarms for DeepSeek V4 Flash. These results show that common inference-time strategies do not provide a reliable solution to the severity-calibration problem.

**Takeaway.** Complementing the main paper’s false-negative study, this analysis highlights a critical LLM failure: the inability to balance detecting fatal violations against preserving valid protocols. Current LLMs act as miscalibrated severity classifiers, struggling to differentiate valid, minor, and fatally flawed protocols. This reinforces PHYSDOX’s core finding: feasibility assessment demands holistic, calibrated reasoning, not superficial keyword matching or verbose rationales.

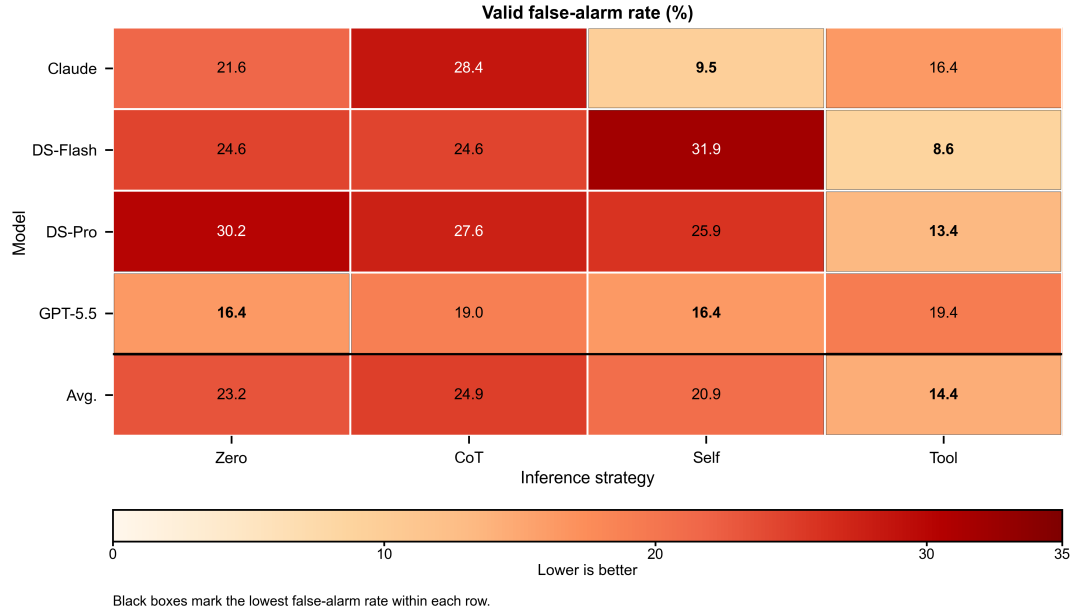


Figure 6: **Valid false-alarm rate across models and inference strategies.** Each cell reports the percentage of Gold-set valid protocols incorrectly predicted as non-valid. Lower values indicate better preservation of feasible protocols. The heatmap shows that false-alarm behavior is highly model- and strategy-dependent.

## D Full Stage-2 Diagnostic Results

This appendix provides the full Stage-2 three-way diagnostic results on the Gold set. The main paper reports a subset of two-stage metrics to highlight the severity-gate bottleneck, while Table 7 expands the Stage-2 diagnosis results with accuracy, balanced accuracy, macro-F1, and Top-2 accuracy under Oracle, Gated, and End-to-End settings.

**Reading the table.** Oracle evaluates diagnosis on all ground-truth fatal-violation protocols, isolating whether a model can identify the coarse physical-error category once the protocol is already known to be fatal. Gated evaluates diagnosis only on the ground-truth fatal protocols retained by Stage-1 fatal gating; Gate N reports the retained count out of 377 fatal protocols. End-to-End evaluates the full two-stage pipeline over all ground-truth fatal protocols and therefore penalizes both missed fatal cases and incorrect downstream diagnosis. Thus, Gated scores should be interpreted as conditional diagnostic performance, whereas End-to-End scores reflect practical protocol-auditing performance.

**Observation.** Table 7 confirms that strong conditional diagnosis does not necessarily translate into reliable end-to-end auditing. Several settings achieve high Gated accuracy or Top-2 accuracy after Stage-1 filtering, but their End-to-End performance remains substantially lower because many fatal protocols are not routed to Stage 2. These results reinforce the main-paper finding that severity-gate calibration, rather than downstream taxonomy classification alone, is the key bottleneck.

This systemic bottleneck is vividly demonstrated by Claude Opus 4.7 (Tool-Augmented), which

Model	Strategy	Gate N	Oracle				Gated				End-to-End			
			Acc.	BAcc.	M-F1	Top-2	Acc.	BAcc.	M-F1	Top-2	Acc.	BAcc.	M-F1	Top-2
GPT-5.5	Zero-Shot	313	50.7	55.0	49.8	85.9	52.1	56.2	51.6	87.2	43.2	48.1	46.6	72.4
GPT-5.5	CoT	293	52.3	55.9	51.0	84.4	53.2	55.9	52.3	84.6	41.4	44.6	45.9	65.8
GPT-5.5	Self-Cons.	316	53.1	57.4	52.8	84.1	54.1	58.4	54.5	85.4	45.4	50.0	49.5	71.6
GPT-5.5	Tool-Aug.	282	56.0	58.9	55.5	86.7	58.2	61.4	58.6	88.7	43.5	46.5	50.1	66.3
Claude Opus 4.7	Zero-Shot	245	58.1	59.3	56.4	91.0	65.3	67.9	64.2	93.9	42.4	44.4	51.3	61.0
Claude Opus 4.7	CoT	217	55.7	55.2	53.2	88.3	65.0	65.8	63.7	90.8	37.4	39.9	48.3	52.3
Claude Opus 4.7	Self-Cons.	255	58.9	59.0	56.6	90.7	65.1	67.0	63.9	95.3	44.0	44.9	51.8	64.5
Claude Opus 4.7	Tool-Aug.	229	63.9	60.5	60.8	92.0	68.1	67.1	66.9	94.3	41.4	42.2	51.6	57.3
DS V4 Flash	Zero-Shot	283	39.0	44.5	36.8	82.0	39.9	45.5	38.2	82.3	30.0	34.2	32.3	61.8
DS V4 Flash	CoT	277	40.3	46.9	38.6	81.7	43.3	49.7	42.6	82.7	31.8	37.0	36.1	60.7
DS V4 Flash	Self-Cons.	301	38.7	44.5	37.4	83.8	41.9	46.7	40.2	86.7	33.4	38.5	35.5	69.2
DS V4 Flash	Tool-Aug.	245	43.5	43.7	40.5	84.6	43.3	47.2	42.5	87.8	28.1	30.1	33.2	57.0
DS V4 Pro	Zero-Shot	215	48.0	54.8	48.3	84.9	50.7	56.7	51.2	87.0	28.9	33.8	37.8	49.6
DS V4 Pro	CoT	223	45.9	50.7	46.2	84.1	49.8	53.6	50.6	87.0	29.4	33.1	37.5	51.5
DS V4 Pro	Self-Cons.	236	46.4	53.9	48.6	87.3	49.6	57.1	52.2	90.7	31.0	36.9	40.4	56.8
DS V4 Pro	Tool-Aug.	169	48.0	51.9	50.2	88.3	53.3	60.2	55.7	88.8	23.9	27.5	34.9	39.8
MiMO v2.5 Pro	Zero-Shot	142	52.0	52.2	49.8	86.7	61.3	62.9	62.5	90.1	23.1	26.3	35.8	34.0
MiMO v2.5 Pro	CoT	152	54.9	56.8	53.9	86.7	61.8	64.4	61.4	87.5	24.9	28.2	37.3	35.3
MiMO v2.5 Pro	Self-Cons.	137	57.0	58.6	55.9	89.9	67.2	70.3	69.3	95.6	24.4	28.3	38.7	34.7
MiMO v2.5 Pro	Tool-Aug.	134	55.4	53.8	53.5	89.1	61.9	63.7	64.3	94.0	22.0	24.6	34.6	33.4
MiMO v2.5	Zero-Shot	144	49.9	55.2	49.9	86.7	56.9	62.8	57.8	88.2	21.8	26.5	34.1	33.7
MiMO v2.5	CoT	163	50.1	53.8	49.3	84.1	57.7	63.1	58.1	87.1	24.9	29.1	36.9	37.7
MiMO v2.5	Self-Cons.	163	52.3	57.1	52.0	86.2	63.2	68.3	64.6	90.2	27.3	32.5	41.1	39.0
MiMO v2.5	Tool-Aug.	154	54.4	51.6	51.5	87.8	59.7	60.2	60.3	89.6	24.4	25.1	35.2	36.6

Table 7: **Full Stage-2 three-way diagnostic results on the Gold set.** Oracle evaluates diagnosis on all ground-truth fatal samples. Gated evaluates diagnosis only on fatal samples retained by Stage-1 gating. End-to-End evaluates the full two-stage pipeline. All metrics except Gate N are percentages.

achieves the highest Gated and Fine-12 oracle metrics yet fails to maintain this advantage end-to-end due to anaemic fatal-gate recall. Consequently, these results provide empirical validation for our two-stage task formulation, confirming that resolving the upstream severity calibration deadlock is far more critical for scientific safety than merely expanding downstream diagnostic vocabularies.

## E Model Selection, Scaling Boundaries, and Silver Provenance

**Selection rationale.** Our goal is not to benchmark every available LLM architecture, but to test whether physical-feasibility auditing failures persist across representative current model families and inference-time strategies. We therefore select six LLM variants spanning multiple provider families, access regimes, and capability levels. The evaluation includes stronger general-purpose models, lightweight or cost-efficient variants, and models evaluated under the same four inference strategies: zero-shot, chain-of-thought prompting, self-consistency, and tool-augmented prompting.

**Model metadata and evaluation roles.** Table 8 summarizes the model coverage used in PHYSDOX. We report only metadata that is available or directly relevant to our evaluation. For models whose exact parameter counts or training details are not publicly disclosed, we mark these fields as undisclosed rather than estimating them. We also distinguish model access from weight inspection: in this study, models are evaluated through their available inference endpoints, and we do not rely on local checkpoint inspection or parameter-level analysis.

Model	Family / regime	Size metadata	Role in evaluation
GPT-5.5	GPT-family hosted model	Undisclosed	Frontier general-purpose LLM
Claude Opus 4.7	Claude-family hosted model	Undisclosed	Strong reasoning-oriented LLM
DeepSeek V4 Flash	DeepSeek-family efficient variant	Undisclosed	Cost-efficient deployment-oriented model
DeepSeek V4 Pro	DeepSeek-family stronger variant	Undisclosed	Stronger same-family comparison point
MiMo v2.5 Pro	MiMo-family stronger variant	Undisclosed	Strong MiMo-family comparison point
MiMo v2.5	MiMo-family lightweight variant	Undisclosed	Lightweight MiMo-family comparison point

Table 8: Model coverage in PHYSDOX. The table documents the role of each evaluated model rather than presenting a parameter-scaling study. Exact parameter counts and training details are marked as undisclosed when they are not publicly available or not directly verifiable from our evaluation setup.

**Why we do not claim a scaling law.** A controlled scaling-law analysis would require a matched family of models with known parameter counts, comparable training data, identical deployment constraints, and sufficiently dense size coverage. The current evaluation does not satisfy these requirements because several API models do not disclose model size, and the evaluated systems differ in training data, alignment procedure, inference stack, and tool-use behavior. We therefore avoid claiming that physical-feasibility auditing is or is not an emergent capability of scale. Instead, our results show that severity-calibration failure appears across the evaluated model families and is not resolved by common inference-time strategies.

**Architecture and domain-specialized models.** Our benchmark does not cover every architecture lineage, such as Llama-family open-weight models, nor models specifically tuned on code, mathematics, physics, or scientific corpora. This is a limitation of the present study. Such models would be informative for testing whether explicit scientific or numerical training improves physical feasibility auditing. We leave this broader architecture and specialization study to future benchmark expansions. The present conclusions should therefore be interpreted as evidence of a persistent failure pattern across the evaluated systems, not as an exhaustive claim over all possible LLM architectures.

**Interpretation boundaries.** The evaluated model suite supports three conclusions. First, physical-feasibility auditing remains difficult for several strong contemporary LLM families under a shared evaluation protocol. Second, the main bottleneck is severity calibration rather than only downstream fatal-error taxonomy classification. Third, common inference-time strategies, including longer rationales, self-consistency, and generic tool augmentation, do not reliably resolve this bottleneck. The evaluation does not support stronger claims about all possible open-weight architectures, all domain-specialized scientific models, or the scaling behavior of physical auditing ability with parameter count.

**Relation to the Silver set.** The Silver set is used for large-scale trend analysis rather than as the basis for safety conclusions. This distinction is important because the Silver release includes targeted MiMo-generated candidates used to fill label and fatal-constraint quotas. All main safety claims are therefore based on the expert-curated Gold set, which is disjoint from the Silver set and is used as the primary benchmark for model comparison.

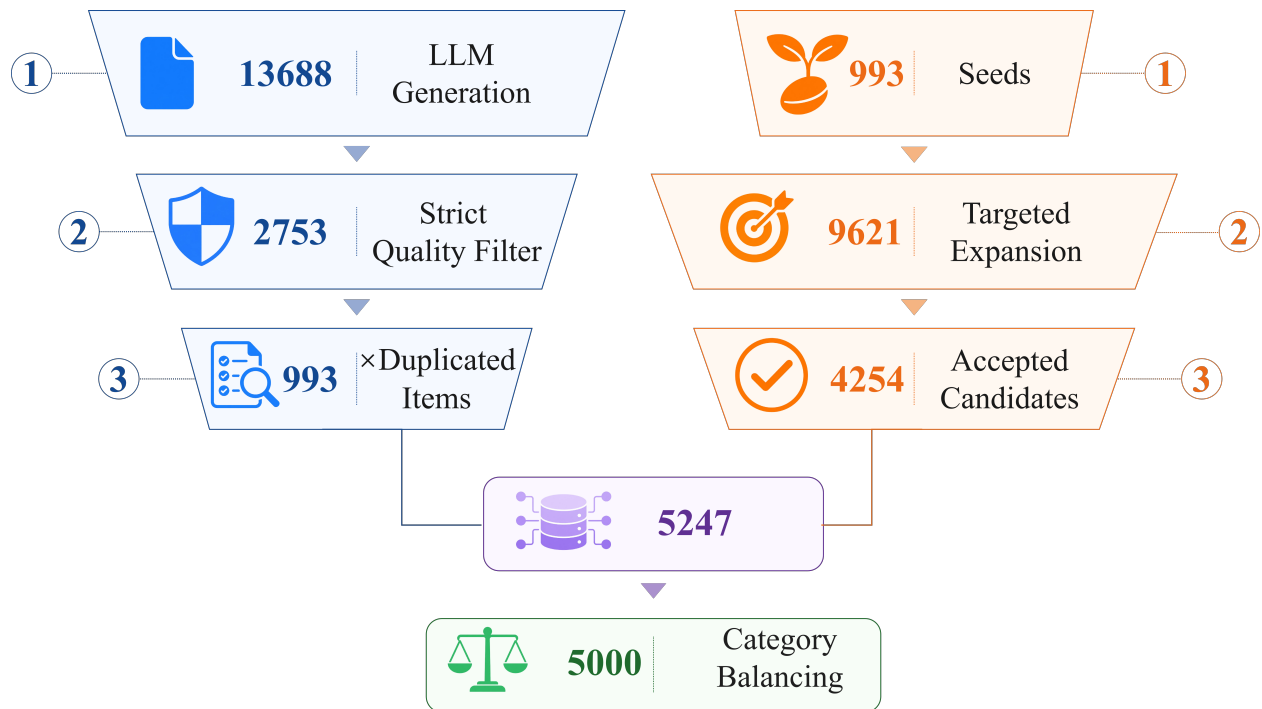


Figure 7: **Silver 5k data curation pipeline.** The pipeline starts from 13,688 candidate protocols, applies strict quality filtering and deduplication, supplements missing quotas through targeted MiMO generation, and freezes the final 5,000-sample Silver release through deterministic quota sampling.

## F Silver 5k Data Curation Pipeline

**Purpose.** This appendix documents the construction of the Silver 5k release. The goal is to preserve only fully specified, unique, hardware-grounded protocols while using targeted generation to fill balanced label and fatal-constraint quotas. The Silver set is therefore not a raw model-generated pool, but a filtered and frozen benchmark split designed for large-scale trend evaluation.

### F.1 Construction Overview

Figure 7 summarizes the Silver-set curation pipeline. We start from 13,688 candidate protocols aggregated from existing Silver candidates and historical generated pools, which include valid, minor-issue, and fatal-violation candidates before strict public-release filtering. We first apply quality and leakage filters to remove protocols with missing mandatory sections, insufficient section content, wrapper text, prompt leakage, placeholder artifacts, or incomplete label metadata. This step retains 2,753 candidates. We then normalize whitespace and remove duplicate protocol texts, reducing the quality-pass pool to 993 unique clean seeds. Because the filtered seed pool is insufficient to satisfy the planned label and fatal-constraint quotas, we perform 9,621 targeted MiMO v2.5 Pro generation attempts to supplement underrepresented labels and constraint categories. This process yields 4,254 accepted generated candidates. The 993 clean seeds and 4,254 accepted generated candidates are merged into a strict candidate pool of 5,247 protocols. Finally, we perform deterministic quota sampling with seed 42 to freeze the final 5,000-sample Silver release.

Stage	Count	Operation	Notes
Initial candidate pool	13,688	Aggregate existing Silver candidates and historical generated pools	Includes valid, minor, and fatal candidates before strict public-release filtering.
Quality-pass raw candidates	2,753	Apply protocol quality and leakage filters	10,935 candidates rejected by the first triggered quality rule.
Unique clean seed pool	993	Normalize whitespace and remove duplicate protocol text	1,760 duplicate protocol rows removed after quality filtering.
Targeted MiMo generation attempts	9,621	Generate valid, minor, and fatal candidates to fill missing label and constraint quotas	MiMo v2.5 Pro with batched targeted generation.
Accepted generated candidates	4,254	Keep generated candidates passing the same quality and uniqueness filters	Computed as 9,621 attempts minus 5,367 rejected attempts.
Strict pool before final sampling	5,247	Combine 993 unique clean seeds with 4,254 accepted generated candidates	Used as the strict unique pool for final quota sampling.
Frozen Silver 5k release	5,000	Deterministic quota sampling with seed 42	Frozen at 2,250 fatal, 1,500 valid, and 1,250 minor samples.

Table 9: **Detailed construction funnel for the Silver 5k release.** The table reports each major curation stage, the number of candidates retained, and the operation applied at that stage.

Rejection reason	Count
<i>Source candidates</i>	
Missing mandatory section headers	5,199
Forbidden wrapper / prompt leakage	3,065
Protocol length below 180 words	753
Weak data acquisition section	663
Weak objective section	658
Other quality or metadata failures	597
<i>Generated candidates</i>	
JSON parse failure	3,381
Protocol length below 180 words	1,832
Weak data acquisition section	82
Forbidden wrapper / prompt leakage	32
Other section-quality failures	40

Table 10: **Main rejection reasons during Silver-set curation.**

## F.2 Quality Filtering and Rejection Analysis

Quality filtering is deliberately strict. Candidates are rejected if they lack mandatory sections, contain wrappers or prompt leakage, are too short, contain weak section content, duplicate another protocol after normalization, or violate label-specific metadata rules. For generated candidates, the same filtering and uniqueness checks are applied before they can enter the strict candidate pool. Table 10 summarizes the dominant rejection reasons.

## F.3 Final Silver-set Composition

The final Silver release contains 5,000 unique protocols with fixed label quotas and broad coverage across six biomedical sensing domains. As shown in Table 11, the release contains 2,250 fatal violations, 1,500 valid protocols, and 1,250 minor-issue protocols. Fatal-violation samples are approximately balanced across the 12 fatal constraint keys, with each key contributing 187–188 samples.

Category	Count	Share
<i>Severity labels</i>		
Fatal violation	2,250	45.0%
Valid	1,500	30.0%
Minor issue	1,250	25.0%
<i>Domains</i>		
IMU motion	1,019	20.4%
sEMG gesture	1,009	20.2%
EEG BCI	827	16.5%
PPG blood pressure	732	14.6%
Radar vital signs	728	14.6%
Throat-microphone speech	685	13.7%

Table 11: **Final composition of the frozen Silver 5k release.** The release contains 5,000 unique protocols with fixed label quotas and broad domain coverage across six biomedical sensing settings.

#### F.4 Cleaning and Generation Rules

**Protocol format validation.** A protocol can enter the strict unique pool only if it satisfies release-level quality checks. Each protocol must contain exactly seven mandatory sections: *Protocol*, *Objective*, *Equipment*, *Sensor Placement & Configuration*, *Data Acquisition Procedure*, *Signal Processing & Validation*, and *Safety & Feasibility*. The protocol must contain at least 180 words, and each section must contain substantive content rather than placeholder text. Protocol text must also be unique after whitespace normalization.

**Leakage and wrapper filtering.** We reject candidates containing wrappers, placeholders, prompt leakage, instruction traces, or benchmark-construction language. Examples include bracket placeholders, “source protocol text”, “procedure below”, “as written above”, “original protocol”, “rewritten protocol”, “I will rewrite”, “output only”, “required headers”, and “benchmark construction”. This filtering is designed to remove model-generation artifacts and ensure that the released protocols resemble standalone experimental methods rather than prompt-completion traces.

**Label-specific metadata validation.** Label-specific metadata is checked before final release. Valid protocols must not retain violation metadata. Minor-issue samples must include complete metadata fields describing the violated best-practice principle, why the protocol remains physically feasible, the minimal fix, and what changed. Fatal-violation samples must be tied to one of the 12 fatal constraint keys. The final release is validated to contain 5,000 unique IDs, 5,000 unique protocol texts, exact label quotas, exact fatal-constraint quotas, no remaining quality issues, no wrapper hits, no bracket-placeholder hits, and no protocols under the minimum-length threshold.

**Targeted MiMo generation.** Targeted MiMo generation is used only after filtering and deduplication, and only to fill missing label or fatal-constraint quotas. Valid, minor-issue, and fatal-violation templates share the same seven-section output format. For fatal-violation, each call is conditioned on a domain, sensors, target signals, typical parameters, a study variant, and one fatal constraint key. The generation prompt requires the protocol to remain fluent and plausible as an experimental methods section while containing exactly one fatal flaw tied to the specified constraint. Generated

candidates are not automatically admitted into the benchmark; they must pass the same quality, leakage, metadata, and uniqueness checks as source candidates.